Friction Identification From Robotic Insertion Tasks

by

Alec Lin
B. Sc in Eng., Beijing Polytechnic University, 1997

A Thesis Submitted in Partial Fulfillment of the
Requirements for the Degree of

MASTER OF APPLIED SCIENCE

in the Department of Mechanical Engineering.

We accept this thesis as conforming
to the required standard

[redacted]

Dr. Inna Sharf, Supervisor (Department of Mechanical Engineering)

[redacted]

Dr. Geoffrey W. Vickers, Departmental Member (Department of Mechanical Engineering)

[redacted]

Dr. Jens Bornemann, Outside Member (Department of Electrical and Computer Engineering)

[redacted]

Dr. Pan Agathoklis, External Examiner (Department of Electrical and Computer Engineering)

Supervisor: Dr. I. Sharf

Abstract

In this thesis, the characteristics of friction and the friction models developed to capture them are presented. An optimization-based friction parameter identification method is proposed, after investigation of friction models and non-linear identification techniques. The identification method is verified through numerical simulation and used to identify friction parameters from experimental data. This synthesized method can also be used to identify parameters for other non-linear models. The friction parameter identification scheme will provide the users of robot simulators, such as the Manipulator Development Simulation Facility (MDSF) an effective approach to obtain contact dynamic parameters from experimental data. The contact parameters and in particular the friction parameters are necessary for simulation, design and mission planning of space manipulator systems.

Examiners:

[redacted]

Dr. Inna Sharf, Supervisor (Department of Mechanical Engineering)

[redacted]

Dr. Geoffrey W. Vickers, Departmental Member (Department of Mechanical Engineering)

[redacted]

Dr. Jens Bornemann, Outside Member (Department of Electrical and Computer Engineering)

[redacted]

Dr. Pan Agathoklis, External Examiner (Department of Electrical and Computer Engineering)

Table of Contents

List of Figures

List of Tables

Acknowledgements

I would like to thank my supervisor Dr. Inna Sharf for her support and patience. I would also like to thank the previous researchers for providing the necessary background and data for this work. Finally, I want to thank my family and friends, whose help and encouragement were instrumental in the completion of this thesis.

To my father and my mother.

Chapter 1

Introduction

1.1 Background and Objective

With the development of modern space techniques, more and more robotic manipulations are proposed for space operations, such as using space robotic arms to assemble the space station, capture satellites, berth and dock various modules, and replace space station components. Most of these important and complex functions involve constrained motions or contact tasks, when the manipulator comes in contact with other objects. Many of these contact tasks can be viewed as insertion operations whereby a robotic arm must insert a particular payload into a mating object. Increasing knowledge of contact dynamics is demanded in order to design and perform more complex tasks during space station operations.

Every manipulator operation on the space station must be first validated by computer simulation and terrestrial simulation to ensure its feasibility and reliability before the risk of performing it in space. During the 1990s, MacDonald Dettwiler

Space and Advanced Robotics (MDR)[1] developed the Manipulator Development and Simulation Facility (MDSF) [16]. It was designed to be capable of providing dynamics simulations of arbitrarily configured robotic manipulator in multi-body contact environment. With MDSF, it is possible for MDR engineers to simulate contact tasks, but the user must supply a number of contact parameters to define the contact dynamics model, including contact stiffness, damping and friction.

The problem for the user, however, is how to choose appropriate values for these parameters? Can they just be values found in engineering handbooks or obtained by some fashion from terrestrial experiments? Can the chosen values match the practical situations of space tasks? Among the three contact parameters, the stiffness and damping terms typically involve a simple linear relationship to motion, and they can be identified with linear identification methods. Contact friction presents a more complicated case: it is highly non-linear and affected by many factors.

The goals of this thesis are: (i) to investigate the effects of friction force on the dynamics and execution of contact tasks; (ii) to validate the friction models and their parametrization; and (iii) to develop and evaluate identification techniques for determining friction parameters.

In 1999, researchers at the University of Victoria (UVic) completed a collaborative research project with MDR titled "Experimental Investigations of Contact Tasks for Space-Based Manipulators" [23]. The purpose of this project was to validate the contact dynamics capability of MDSF. In the course of the validation project, a large database of experimental results was generated. This data was obtained using the

[1]MD Robotics was formed May 1999 following acquisition of the former Spar Space Robotics operation from Spar Aerospace Limited.

planar robotics test bed and a special-purpose contact dynamics interface in a series of peg-hole insertion/removal experiments. On the other hand, the experimental configuration in the test-bed was modeled and defined as input to MDSF. The output of MDSF, the dynamics simulation results, was compared to the experimental results from the test-bed. Their accordance and disagreement were analyzed to validate the contact dynamics capability in MDSF.

As discussed above, in order to model contact tasks in MDSF, the user must supply the contact parameters including contact stiffness, damping, and friction. In the aforementioned project these parameters were either guessed or estimated in some fashion. In 2000, a master's thesis on contact stiffness and damping estimation was completed by Erickson [9]. The force tracking strategy within adaptive control was applied to determine stiffness and damping successfully.

The principal motivation for the present work, however, stems from the need to have a more reliable means of identifying friction between contacting bodies from measurements collected during real operations of space manipulators. Because the general linear identification method cannot be used to identify non-linear model, such as friction, a non-linear approach is considered.

1.2 Historical Perspective and Literature Review

The earliest friction model, friction force being proportional to the normal load, opposing the motion, and independent of contact area, was known to Leonardo da Vinci in 1519 [18]. This conclusion remained hidden in his notebooks for centuries until rediscovered by Amontons in 1699. This model was developed by Coulomb in 1785 and recognized by the scientific field at that time. Morin (1833) introduced the idea

of static friction, and Reynolds (1866) discovered the equation of viscous fluid flow, completing the friction model that is most commonly used in engineering:

$$total\ friction = static\ friction + Coulomb\ friction + viscous\ friction. \quad (1.1)$$

Tribology, which in Greek means "the study of rubbing", was born in England in the 1930s. The basic problems of wear in mechanisms, true contact area, relationships between friction, material properties and lubrication processes were addressed and answered. Today tribology is concerned with three major issues: rubbing, lubrication, and wear.

In mechanisms, friction can cause errors in position regulation and tracking lag. These errors can be reduced by using proper lubrication, or further compensated by model-oriented control techniques. However, the friction happening during impact or contact is difficult to predict and measure. An extensive survey on friction phenomenon and modelling was carried out by Armstrong *et al.* in 1991 [1], and most of important concepts and features of friction are included in this survey report.

1.2.1 Microscopic View of Contacting Surfaces and Dry Friction

Let us consider two bodies in contact with their surfaces finished with high precision. In a microscopic view, as shown in Figure 1.1, the pair of contact surfaces are not as flat and smooth as their macroscopical view, but built up of small asperities on each of their surfaces.

The assumption is that the actual contacts of these asperity junctions are the major cause of friction when relative motion occurs between the contact surfaces. In

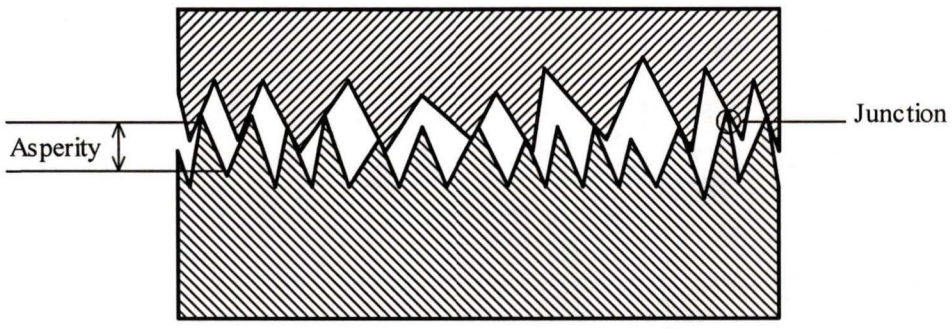

Figure 1.1: Microscopical View of Asperity Junctions

engineering materials the slopes of the asperities are typically 5 to 10 degrees, whereas the junction widths are typically $10^{-5}m$ for steel. The true area of contact is therefore much smaller than the apparent area of contact.

Dry friction is friction between two bodies in the absence of contamination of the contact surfaces [1]. This abstract situation is impossible to achieve in a real mechanical system due to the fact that chemical reactions will occur at the surfaces and create oxide films. However, major characteristics of friction are determined according to the conditions of this ideal case where:

$$Friction\ force = (true\ area\ of\ contact) \times (shear\ force\ per\ unit\ area) \quad (1.2)$$

1.2.2 Influence of Lubrication

When the lubrication is available, which is the ordinary case, it will form a thin film between the contact surfaces [3] [1]. It is common to define four different regimes for friction as a function of velocity as shown in Figure 1.2 and described below :

I *Static friction and pre-sliding displacement*

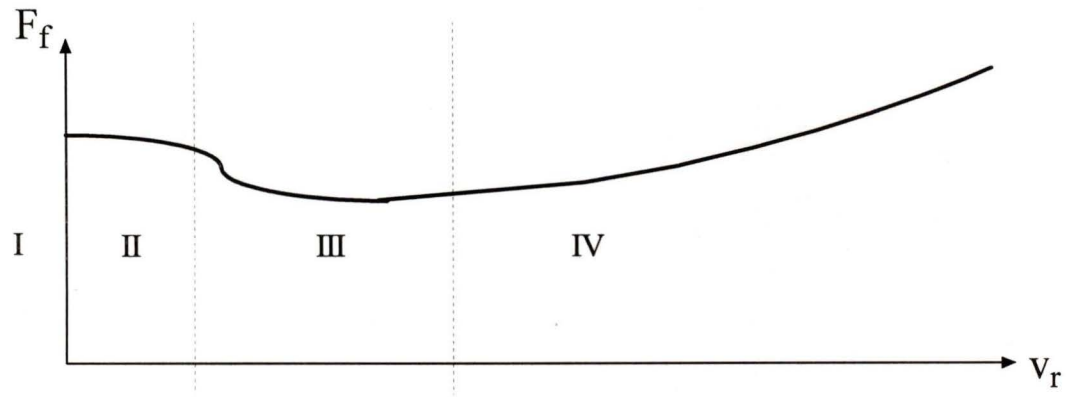

Figure 1.2: Friction vs Velocity in Steady State

This is the initial regime with contact taking place between asperity junctions with only a very thin film at the junctions. Elastic and plastic deformations of asperities generate shear force between the contacting objects where potential relative motion exists. When velocity is zero, the friction force can take on multiple values and the pre-sliding displacement is proportional to the applied external force. For sufficiently large displacements the asperity junctions break away and the contact surfaces start sliding against each other.

II *Boundary lubrication*

For very low velocities, no fluid film is present between the surfaces, and the forces acting at the interface are pure shear forces of solid boundary films.

III *Partial fluid lubrication*

In this regime lubricant is drawn into the junction interfaces, and due to the viscosities some of the lubricant creates a fluid film between the contacting surfaces.

However, the film thickness is thinner than the size of the asperities, and therefore some of the load is carried by the lubrication film, and some by elastic and plastic deformation of the asperities. As the velocity increases, the film thickness increases; the resulting tangential force decreases since the shear forces of the lubricant film are smaller than the shear forces of the asperities. This is referred to as the *Stribeck effect.*

IV *Full fluid lubrication*

In this regime a lubricant film thicker than the size of the asperities is maintained. The friction characteristics are now determined by hydrodynamic or elasto-hydrodynamics theory. In the hydrodynamic case there is only viscous friction. The viscous friction increases with velocity since the shear rates and the shear strengths of the fluid film are proportional to sliding velocity.

1.2.3 Friction Related Phenomena

The friction between contacting bodies is in fact a complex phenomenon composed of several different physical phenomena in combination. The influential factors on these components are contact geometry, the properties of the materials of the bodies, the presence of contaminants (lubrication) on the contact surfaces, and also the relative motion of the bodies. In general, there are seven different elements and related effects of friction as described below [1]:

1. *Kinetic friction* or *Coulomb friction.*

This the simplest form of friction and it can be written in the form of a single function as in (1.3). It was first discovered by Coulomb [3] and denoted as *kinetic*

friction as it defines friction for non-zero velocities in the form:

$$F_f = F_k \operatorname{sgn}(v_r) \tag{1.3}$$

where F_f is the friction force, F_k is the kinetic friction force, and v_r stands for relative velocity. The kinetic friction, or Coulomb friction, is considered a basic component of the friction force.

2. *Viscous friction.*

The friction force in lubricated systems has a velocity dependent term originating from hydrodynamic effects. This component of friction is modeled with the linear relation

$$F_v = \beta v_r, \tag{1.4}$$

where F_v is viscous friction, β is the viscous coefficient and v_r stands for relative velocity. More generally, viscous friction exhibits a non-linear behavior as

$$F_v = \beta \left| v_r \right|^{\delta_v} \operatorname{sgn}(v_r), \tag{1.5}$$

where parameter δ_v is defined as $\frac{1}{3}$, $\frac{2}{3}$ or 1 depending on the application geometry [1].

3. *Stiction and stick-slip motion.*

It was experimentally discovered that to bring a system from zero velocity to motion, a higher force is needed than to maintain a steady-state velocity. Letting F_e denote the external force and F_s the static friction force, we have

$$F_f = \begin{cases} F_e, & \text{if } v = 0 \text{ and } |F_e| \leqslant F_s; \\ F_s \operatorname{sgn}(F_e), & \text{if } v = 0 \text{ and } |F_e| > F_s. \end{cases} \tag{1.6}$$

The static friction is shortened as "*stiction*". It is difficult to determine the value of stiction precisely as the friction force is not a function of velocity when $v = 0$.

The stiction is the major cause of the stick-slip motion, which is a typical phenomena that occurs in system with friction. The stick-slip motion can be observed experimentally by pulling a spring attached to a block on a rough surface. The block starts to move when the spring is extended so much that the string force exceeds the break-away friction force or the maximum stiction. The motion stops when the spring is compressed. The net result to the block is a jerky motion which switches between sticking and slipping. The stick-slip also occurs when a chalk is drawn at a proper speed on a blackboard and a squeaky noise is created.

4. *Pre-sliding displacement*, also referred to as the "*Dahl effect*".

From experimental observations of friction in small rotations of ball bearings, Dahl discovered that there exists a minor displacement during stiction for small motions at contacting point, which is called *pre-sliding displacement.* The junction behaves like a spring and the displacement is an approximately linear function of the applied external force, up to the critical static friction force. The value of pre-sliding displacements for steel is less that 2 microns. The physical expression of pre-sliding displacement can be obtained from the stress-strain characteristics of the asperity junctions[6].

5. *Static friction dependence on dwell time.*

It has been suggested that the magnitude of static friction is dependent on the length of time (i.e. the "*dwell time*") that the surfaces are at rest during a stick-slip motion. The longer the dwell time, the higher the static friction from kinetic friction F_k up to F_s.

6. *Stribeck effect.*

This term refers to the friction variation with velocities. With low velocities, friction decreases with increasing velocity; this happens during the beginning of lubrication regime III, as shown in Figure 1.2. The simple explanation is inadequacy of lubrication at the lowest velocities. Consider the situation when the slip just begins, and the velocity is too low to produce a fluid layer between the contacting surfaces. Then the friction at the lowest velocities is larger than that at the slightly higher velocities.

7. *Frictional lag.*

From experimental results for the dependance of friction force on variations in velocities, it has been discovered that the magnitude of friction force during decreasing velocities was smaller than the friction force during increasing velocities. The difference between the lower friction force during decreasing velocities and the higher friction force during the increasing velocities becomes larger when the change in speed is more significant.

1.2.4 Time Dependent Properties

There are two major time dependent properties of friction: I. *Rising Static Friction with Increasing Dwell Time* and II. *Frictional Memory.* They refer to the fact that in partial fluid lubrication regime, friction is dependent upon velocity and load; a change in friction will cause lag changes in the velocity of the load.

Other than the above-mentioned properties, features and characteristics of friction, it must be emphasized that the current thesis focuses on the friction force in

contact dynamics. This is much more difficult to determine, as there is almost no steady state motion in contact surfaces but impact and rubbing. The contact parameters are also influenced by many factors, and the direction and values of friction may change from time to time.

1.3 Thesis Outline

In Chapter 1, the background and motivation for this project were introduced. The phenomena and characteristics associated with the non-linear features of friction were introduced in the literature review.

In Chapter 2, friction modelling is addressed. The microscopic view of contact topography is presented. The friction models are classified and their formulations are given together with the physical interpretations and description of the typical features.

In Chapter 3, a simulation of a simple mass-spring system is used in order to validate the friction models introduced in Chapter 2. The results from various friction models are presented and assimilated. This system is a typical example in which stick-slip motion is expected with proper implementation of friction model and appropriate parametrization.

In Chapter 4, the theory and derivation of non-linear parameter identification method is presented. The general procedure for the optimization-based parameter identification scheme is discussed and formulated for different friction models in a simple example. The identification scheme is further verified numerically for this the simple case.

In Chapter 5, the method is applied to one of the most practical constrained

robotic tasks – the insertion of a peg into a hole, where the friction parameters of the bristle model are identified from the data collected in the previous project [24]. The data used for parameter identification procedure were obtained from real experimental contact tasks conducted on the UVic Robotics Test-bed. The results are presented and compared to the values obtained with other approaches.

In Chapter 6, conclusions and thesis contributions are discussed. Future research on contact dynamics parameter identification is suggested.

Chapter 2

Friction Modelling

2.1 Background

Friction models used in mechanism simulation and control algorithms can be classified into two major categories. The first category is the traditional *static models*, the other is that of the modern *dynamic models.*

For decades, friction was modelled as a static map from relative velocity at a contact point to a value less than normal force at the contact point. These are the traditional static friction models. In these models, the friction force is a function of instantaneous relative velocity between contacting surfaces. The sign of the friction force depends on the sign of the velocity, and the magnitude of friction may be the sum of static, kinetic, and viscous components. However, there are several interesting properties observed in systems with friction that cannot be explained solely by traditional static models. This is basically due to the fact that friction does not have an instantaneous response to a change of velocity, i.e. it has internal dynamics. Examples of these dynamic properties are stick-slip motion, pre-sliding displacement,

the Dahl effect, and frictional lag, which were introduced in Chapter 1.

To capture the above-mentioned dynamical characteristics, various modern dynamic friction models have been proposed by researchers since the 1960's to meet different requirements of friction modelling. Dahl proposed his model, which includes a mechanism for zero velocity sticking in 1968 [6]. Subsequently, several friction models completely different from the traditional static models were developed and used in mechanical transmission, control simulation, and system identification. The motivation for developing new models stemmed from the demand for simplicity and accuracy of representing the complicated friction features.

The advantage of dynamic models came from their continuity and stability. It was assumed that the friction force between two contacting surfaces was caused by the tangential conjunction between them, i.e., the virtual *bristle* [11]. The original integrated variable in Dahl's model was not associated with bristles but the asperities, or the peaks and valleys in a microscopic view.

In these models, the main component of the friction force is stiffness multiplied by an integrated variable representing bristle deflection. Additional terms including increment of stiction, damping, and viscous friction are included as functions of the integrated variable, which is generally associated with relative velocity. This kind of model is good for presenting some of the complicated phenomena associated with friction such as stick-slip motion, which cannot be captured with the velocity-based models. These models include Dahl's model [1], the Bristle model [11], the LuGre model [7] and other integration based models. In these models, the friction force is a function of state variables, in particular, the relative velocity and displacement at the contact point.

The static and dynamic models have different characteristics, some of which are

suitable for the design of model-based friction compensation schemes, while some can be advantageous for simulation of contact dynamics, e.g., the robotic manipulator grasping an object. For either static or dynamic models, the primary concern of friction modelling is accuracy, because they are often used to compensate the friction force to achieve the desired motion in a mechanism. The secondary concern of these models is continuity and stability at low velocities. Computer systems usually have difficulties in treating very small numbers; therefore the continuity of friction values at small velocities is often difficult to model. In fact, it is not feasible to use the condition of equality to zero to switch between zero and non-zero velocities in the computer-based models. Other concerns in modelling include stability and efficiency, both of which ensure the feasibility of computation.

An ideal friction model should cover all the frictional characteristics discovered to date, including the different features during the four lubrication regimes, the seven friction components, and two time-dependent properties, as summarized in Chapter 1. However, a model addressing all aspects of the friction phenomena would be too complex. As a matter of fact, a particular friction model will focus on the most important features of the friction phenomena, such as stick-slip and Stribeck effect.

One complex 7-parameter model, which includes most of the above-mentioned features, was proposed by Armstrong [1] and was regarded as the ultimate static model. The 7-parameter model actually contains several models, which are used depending on the particular situation. The mathematical formulation of the model takes the form of a polynomial containing several non-linear terms, each representing a typical frictional feature. One component of the model will judge the motion and then switch the effective terms on and the ineffective terms off. Though the model is powerful in modelling friction, the usage of this kind of model is limited to theoretical

and analytical research only. In fact, parameter estimation represents one of the most serious concerns associated with the usage of very complicated friction models. The 7-parameter model is seldom used in practical applications, as it is difficult to identify all parameters simultaneously with a single identification algorithm.

In the following sections of this chapter, several typical friction models in both categories will be discussed and investigated. These friction models are worth consideration as they are capable of capturing the majority of important characteristics of friction. Furthermore, these models are not exceptionally complicated in terms of parameter identification problem. All the parameters of the friction models are named with their original notation though they have the similar physical meaning.

2.2 Static Friction Models

The earliest friction model was defined by Leonardo da Vinci in the sixteenth century [18]. As further friction related phenomena were discovered during the development of the fields of physics and mechanics, an expanding number of terms were added to the friction models to cover these features. In this fashion, the static models were formed and developed until they reached the state of the most recent 7-parameter model.

In general the static friction models can be regarded as combinations of Coulomb, viscous, and static frictions, and their extensions. Figure 2.1 shows several static friction models, from upper left to right: Coulomb model, Coulomb friction + stiction, Coulomb friction + stiction + viscous friction, Coulomb friction + stiction + viscous friction + Stribeck effect. In the following sections, the classical model, Karnopp

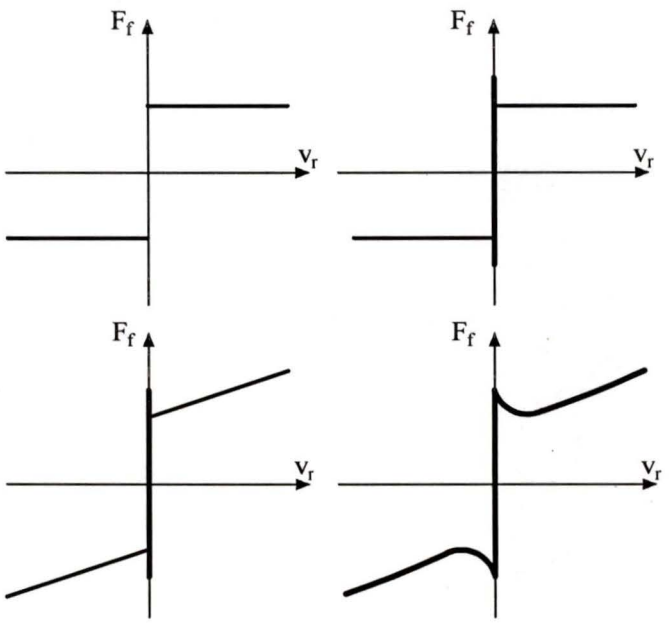

Figure 2.1: Traditional Static Models

model and the 7-parameter integrated model are presented and discussed.

2.2.1 Classical Model

The Classical model was designed to make the velocity-friction relationship continuous, which is easy to both implement numerically and simulate in time. The assumption behind the model is that friction force is linearly related to the relative velocity of the contact point for different speed regimes, as shown in Figure 2.2 and defined below:

$$F_f = \begin{cases} \frac{F_1}{v_1} v_r, & \text{if } v_r < v_1 \\ F_2 + \frac{F_1 - F_2}{v_1 - v_2} v_r, & \text{if } v_1 < v_r < v_2 \\ F_2, & \text{if } v_r > v_2 \end{cases} \tag{2.1}$$

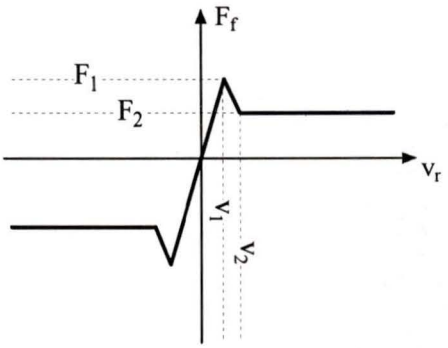

Figure 2.2: Classical Model

From the figure, we can see that F_2 is the sliding friction force. When the relative velocity v_r is larger than v_2, the friction force turns out to be sliding friction.

This model attempts to include stiction by increasing friction values in low velocity regimes, i.e., when $v_1 < v_r < v_2$, the friction values of F_f are between the maximum stiction F_1 and sliding friction force F_2. During stiction, when $v_r < v_1$, the friction force can resist the external force in the opposite direction with the magnitude as a function of v_r up to the peak stiction force; if the external applied force exceeds F_f the system will begin to accelerate. However, in this model the friction force F_f generated by the system is a function of relative velocity v_r, and independent of the external applied force.

Simulation results presented in the Chapter 3 will show that this model can exhibit the stick-slip phenomenon during certain velocity regimes when v_1 and v_2 are chosen as very small numbers. In this thesis, this model was used to simulate a simple mass-spring system moving on a rough surface in §3.1.2 and to test the non-linear parameter identification algorithm in §4.3.1.

2.2.2 Karnopp Model

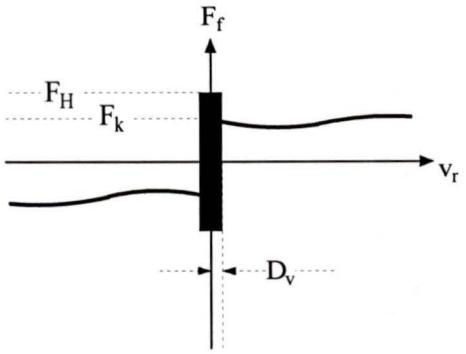

Figure 2.3: Karnopp Model

The Karnopp model was first proposed in [13]. It can be viewed as a combination of the extended static friction model plus the kinetic friction model. The friction force F_f is a function of relative velocity v_r and somehow dependent on the sum of externally applied forces, F_e, as shown in Fig. 2.3. A region of small velocity is defined as $[-D_v < v_r < D_v]$, so that inside this region the relative velocity can be regarded as zero. Outside this region, F_f can be an arbitrary function of v_r, while in this thesis a constant kinetic friction value F_k is used. Thus, the model is defined with the following equations:

$$F_f = \begin{cases} F_e, & \text{if } |v_r| \leqslant D_v \\ F_k, & \text{if } |v_r| > D_v \end{cases} \tag{2.2}$$

where inside the $v_r = 0$ region, F_f is determined by the external force F_e applied on the system until the break-away value of stiction force F_H is reached.

According to the original paper by Karnopp, the friction force outside the $[-D_v < v_r < D_v]$ regime can be a more complex function of state variables, e.g., a viscous

term can be added to include velocity dependent features. In the present thesis, that function is defined as a constant for the sake of simplicity.

2.2.3 7-parameter Integrated Model

As mentioned in the beginning of this chapter, there is no theoretically motivated model available for all the different components of friction, but some empirically motivated forms have been proposed. For modelling of simple contact dynamics cases, such as sliding between hard metal parts with lubrication, a seven parameter model proposed by Armstrong [1]. This model is sufficient to cover all the friction characteristics, which were discussed in §1.2.3.

The formulation of this model is described in several stages as follows.

Not Sliding Stage: the instantaneous friction force F_f is linear with the so-called pre-sliding displacement x,

$$F_f(x) = -x/k_t \tag{2.3}$$

where k_t is the tangential stiffness coefficient of the static contact, which depends on the properties of the contacting surfaces.

Sliding Stage: the friction force F_f sums up Coulomb, viscous, and Stribeck friction:

$$F_f = -\left(F_c + F_v|\dot{x}| + F_S(\gamma, t_2)\frac{1}{1+\left(\frac{\dot{x}(t-\tau_L)}{\dot{x}_s}\right)}\right)\mathrm{sgn}(\dot{x}) \tag{2.4}$$

where F_c is the Coulomb friction force, F_v is the viscous friction force, F_S is the magnitude of the Stribeck friction, γ is the temporal parameter of the rising static friction, t_2 is the dwell time, i.e. time spent at zero velocity, τ_L is the time constant of frictional memory, $\dot{x}_s$ is the characteristic velocity of the Stribeck friction.

Rising static friction: the break-away static friction level will increase with dwell time according to:

$$F_S(\gamma, t_2) = F_{S,a} + (F_{S,\infty} - F_{S,a}) \frac{t_2}{t_2 + \gamma}. \tag{2.5}$$

where $F_{S,a}$ is the magnitude of the Stribeck friction at the end of the previous sliding period, $F_{S,\infty}$ is the magnitude of the Stribeck friction after a long time at rest.

In this 7-parameter model, the dependent variables are defined as follows:

F_f is the instaneous friction force;

F_S is the magnitude of the Stribeck friction;

$F_{S,a}$ is the magnitude of the Stribeck friction at the end of the previous sliding period;

t_2 is the dwell time, or duration of time at zero velocity.

The parameters for this model are defined as follows:

F_c is the coulomb friction force, the same as in previous models;

F_v is the viscous friction force;

$F_{S,\infty}$ is the magnitude of the Stribeck friction after a long time at rest;

k_t is the tangential stiffness of the static contact;

$\dot{x}_s$ is the characteristic velocity of the Stribeck friction;

τ_L is the time constant of frictional memory;

γ is the temporal parameter of the rising static friction.

In this model, each of the seven parameters is designed to capture a particular friction feature and they are independent of each other. The values of these parameters vary with different contact situations, which depend on the structure of the mechanism, materials of contacting surfaces, and lubrication conditions. However, this model can be used for accurate simulation of the friction phenomena when given appropriate parameter values.

The difficulties of parameter identification for this model arise from two facts: one is that it is difficult to identify these parameters through traditional measurements, especially those parameter values directly related to the magnitude of friction force, F_C, F_v, $F_{S,\infty}$. The other is that these parameters appear in nonlinear combinations. The primary source of these parameter values is the empirical data.

Kim and Lee's research group presented several papers addressing simulation and identification of this model [4] [14] [15]. They investigated parameter identification for this model with "Evolution Strategies", which is a genetic numerical method. By using the identified parameters they defined gains for the robust compensation scheme and implemented the control scheme in a precise ball-screw type positioning table. The identification results were used to compensate the motion error, and the desired motion was achieved and stability was ensured.

2.3 Dynamic Friction Models

As discussed in §2.1, dynamic friction models are those models that have the main component of bristle deflection, plus additional terms of damping and viscous friction. The dynamic models are continuous at zero velocity, and have greater stability. In this section, we present four dynamic friction models: the original bristle model, a modified bristle model implemented in the MDSF, the reset integrator model, and the LuGre model.

2.3.1 Bristle Model

The Bristle model was first introduced by Haessig and Friedland [11]. The contacting surfaces are like two brushes with a large number of bristles on each of them. During the relative motion, the friction is generated by the resistance of the interacting pair of bristles, as shown in Figure 2.4. The assumption is that the material surfaces are not totally flat and smooth but always have some microscopic asperities. According to the definition of the Bristle model, the bristles on each contacting surface take the form of *uniformly distributed*, i.e. the distance between bristles is a random variable having statistic properties consistent with the macroscopic friction characteristics.

When relative motion occurs between the surfaces, a bristle on the upper surface may attach to the bristle on the lower surface and they will form a bristle bond. The friction between the two surfaces is caused by the relative resistance between these bristle bonds, each contributing a small portion to the total friction load.

The tangential resistance force generated by the bristle bond at "A" can be calculated as

$$F_A = k_b(x_A - b_A),$$

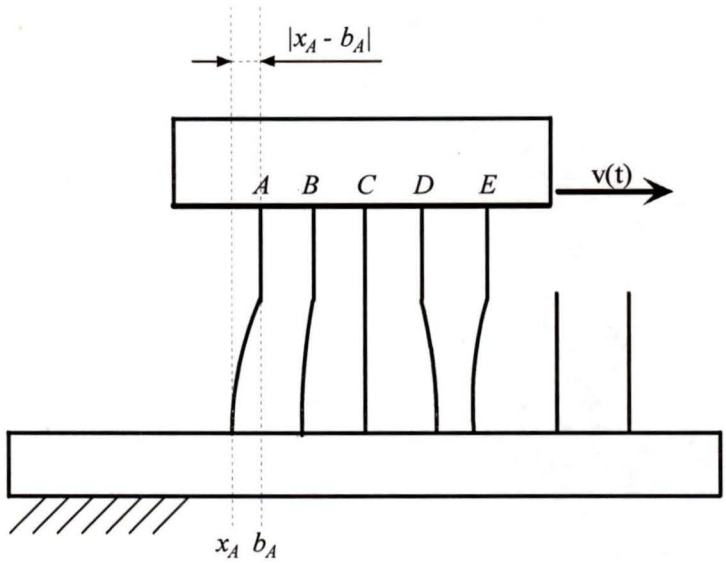

Figure 2.4: Microscopic View of Bristle Contact

where k_b is the stiffness coefficient and $(x_A - b_A)$ is the deflection of the bristle "A". Then the total friction load contributed by each bristle bond is defined as the strain multiplied by a stiffness coefficient, as follows:

$$F_f = k_b \sum_{i=1}^{n} (x_i - b_i),$$

where n is the number of bristle bonds, and $(x_i - b_i)$ is the deflection of the i_{th} bristle, which is defined by the difference of upper bristle displacement x_i and lower bristle position b_i.

When the strain of any particular bristle exceeds a certain level, the bond is broken and a new bond with less strain is established. The number of bristles can be a function of relative velocity, and will directly affect the overall friction load. Therefore the friction load can be made velocity dependent by varying the number of bristles.

The idea behind the bristle model is straightforward enough to understand but the implementation of this model is not trivial. A random number generator is needed to calculate the distribution of bristles at each time step of simulation; when one bond is broken for the upper bristle, the new location of another lower bristle capable of having a new bond established will be calculated. This procedure makes the implementation somewhat complicated.

2.3.2 Modified Bristle Model Used in MDSF

Researchers at MDRobotics have modified the original Bristle model as described in [16]. Their model represents an extension of the Bristle model to the more general three dimensional case. In this model the friction coefficient μ is used to relate the friction force and the normal contact force. The friction force vector $\mathbf{F}_f$ is calculated as

$$\mathbf{F}_f = -k_f \mathbf{s} \tag{2.6}$$

where k_f is the contact bristle stiffness and $\mathbf{s}$ is the vector of the bristle displacement, calculated as

$$\begin{aligned} \mathbf{s}(t) &= \begin{cases} \mathbf{s}(t_0) + \int_{t0}^{t} \mathbf{v}_t dt, \text{ if } |\mathbf{s}| < s_{\max} \\ s_{\max} \dfrac{\mathbf{v}_t}{|\mathbf{v}_t|}, \text{ otherwise} \end{cases} \\ s_{\max} &= \frac{\mu \, |\mathbf{F}_n|}{k_f} \end{aligned} \tag{2.7}$$

In the above, the times t and t_0 are, respectively, the current time and the start time of the last sticking at the contact point; $\mathbf{v}_t$ is the relative tangential velocity between the two contacting bodies at the contact point. The other variables and parameters are listed in Table 2.1.

Note that according to this model, $\mathbf{s}_{max}$ is time-varying since it depends on the normal load $\mathbf{F}_n$ which will in general vary with time. As t_0 is different for each individual contact point, it must be reset for each new impact or each new sticking. Also, the model implicity assumes only one bristle.

Since originally formulated, the friction model used in MDSF has been further augmented to include the damping terms. Since this model has not been published in open literature, we cannot present its exact parametrization here, other than to say that it appears to be very similar to the reset integrator model introduced in the next subsection.

2.3.3 Reset Integrator Model

The Reset Integrator Model was developed to reduce the computational time requirements of the Bristle model while retaining its capacity to accurately represent the stick-slip friction phenomenon.

In this model, a single position variable p is used to represent the average bristle deflection and it can produce the bonding effect of stick-slip friction when sticking. The Reset Integrator Model is defined as follows:

$$\begin{aligned} \dot{p} &= \begin{cases} 0, & \begin{cases} \text{if } v_r > 0 \text{ and } p \geq p_0 \\ \text{if } v_r < 0 \text{ and } p \leq -p_0 \end{cases} \\ v_r, & \text{otherwise} \end{cases} \\ F_f &= k_r p + \beta \dot{p} + a k_r p(|p| < p_0) \end{aligned} \tag{2.8}$$

where the parameters of this model are listed in Table 2.1 and compared to the original bristle model. The block diagram of the Reset Integrator model is shown in Figure 2.3.3.

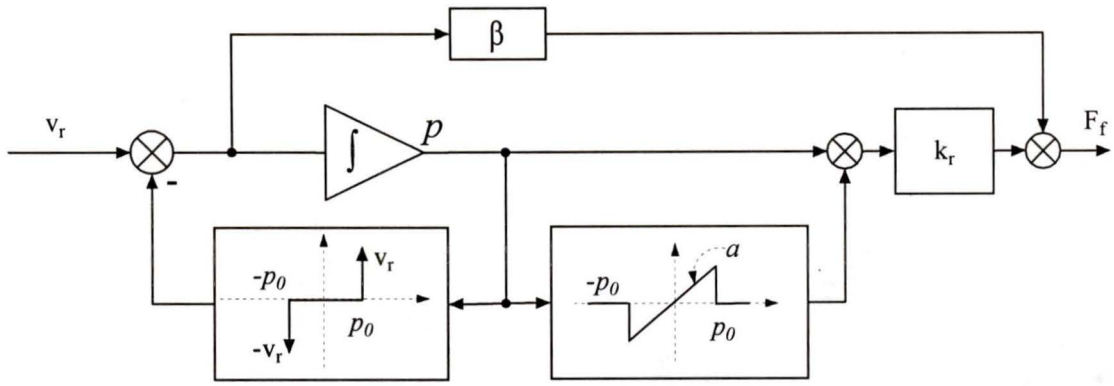

Figure 2.5: Reset Integrator Model

The input to the model is the relative velocity v_r between the contacting surfaces. First, v_r is compared to the output of a nonlinear block that has the effect of turning off the input to the integrator if the current bristle deflection is larger than maximum deflection. Secondly, the position variable p is multiplied by the spring stiffness k_r to determine part of the friction load F_f. A damping term $\beta\dot{p}$ is also included for physical realism. Oscillations are expected to occur after the system has entered into a sticking mode for a relatively short while. The integration of p usually occurs during the sticking phase while the stiction friction force increases with no motion. If there is sliding, the friction force remains constant with no change in magnitude of bristle deflection, which implies the input to the integrator $\dot{p} = 0$.

Reset integrator model captures the same features as the original Bristle model but it has a simpler parametrization and is easier to compute. Table 2.1 presents a comparison of the three dynamic friction models.

Table 2.1: Comparison of Dynamic Friction Models

Model	Original Bristle Model	MDSF friction model	Reset Integrator Model
Description	$b_i = b_i + \text{uniform}(\Delta)\,\text{sgn}(\delta_i)$ $\delta_i = x_i - b_i$ $F_f = F_f + k_b(x_i - b_i)$	$\mathbf{F}_f = -k_f \mathbf{s}$ $\mathbf{s}(t) = \begin{cases} \mathbf{s}(t_0) + \int_{t0}^{t} \mathbf{v}_t dt, \text{ if } \lvert\mathbf{s}\rvert < s_{\max} \\ s_{\max} \frac{\mathbf{v}_t}{\lvert\mathbf{v}_t\rvert}, \text{ otherwise} \end{cases}$ $s_{\max} = \frac{\mu \lvert\mathbf{F}_n\rvert}{k_f}$	$\dot{p} = 0 \begin{cases} \text{if } v_r > 0 \text{ and } p \geq p_0 \\ \text{if } v_r < 0 \text{ and } p \leq -p_0 \end{cases}$ $\dot{p} = v_r, \text{ otherwise}$ $F_f = pK_r + \beta\dot{p} + apK_r(\lvert p\rvert < p_0)$
Variables	F_f total friction load x_r relative position (displacement) i bristle index (i=1:n) n number of bristles (20~50) δ_i deflection of bristle i b_i location of bristle i	$\mathbf{F}_f$ friction force $\mathbf{s}$ vector of the bristle displacement $\mathbf{F}_n$ vector of normal contact force $\mathbf{v}_t$ tangential relative velocity $s_{\max}$ maximum bristle deflection.	F_f total friction load p bristle deflection $\dot{p}$ differential of bristle deflection v_r relative velocity
Parameters	Δ new bristle range k_b spring rate (bristle stiffness) δ_s snapping point N number of bristles	k_f contact bristle stiffness μ the friction coefficient	p_0 maximum bristle deflection K_r spring rate (bristle stiffness) a stiction gradient β dampling coefficient

2.3.4 LuGre Model

The LuGre model was proposed by Canudas de Wit and Olsson [7], and an extensive investigation on this model has been carried out in [10]. The model is used for simulation and comparison to other models in this thesis, and is summerized below.

The formulation of the model is as follows:

$$\begin{aligned}
\frac{dz}{dt} &= v - \frac{|v|}{g(v)}z, \\
z_{ss} &= \frac{v}{|v|}g(v) = g(v)sgn(v), \\
g(v) &= \frac{F_C}{\sigma_0} + \frac{F_s - F_C}{\sigma_0}e^{-(\frac{v}{v_s})^2}, \\
F &= \sigma_0 z + \sigma_1\frac{dz}{dt} + \sigma_2 v, \\
F_{ss} &= F_C sgn(v) + (F_S - F_C)e^{-(\frac{v}{v_s})^2}sgn(v) + \sigma_2 v;
\end{aligned}$$

where the variables are:

z	average deflection of bristles,
v	relative velocity,
$g(v)$	positive function;

and the parameters are:

v_S	Stribeck velocity,
σ_0	stiffness coefficient,
σ_1	damping coefficient,
σ_2	viscous friction coefficient,
F_C	Coulomb friction,
F_s	stiction force.

The successful application of any model relies on the quality of the estimated friction parameters. These parameters are difficult to estimate since they appear in the model in a highly non-linear fashion. It is thus important to investigate identification methodologies to derive a nominal friction model to be used for simulation of real tasks. This subject is addressed in Chapter 4 of this thesis.

Chapter 3

Simulation of Friction Models

It is important to verify the friction models presented in the previous chapter to see if they can convincingly demonstrate friction response in the simulations of dynamic systems. In the following sections, the different friction models are implemented for a simple mass-spring system moving on a rough surface, which has been used to verify friction models since Karnopp [13]. Even though this system is very simple, it exhibits one of the most important features of frictional dynamics – the stick-slip motion at low velocities. This system has also been used by several researchers as a benchmark test to evaluate the efficiency of friction models [11] [1]. Several friction models from Chapter 2 will also be evaluated by using a more complex example consisting of two springs and two bodies, one of which is under two-point contact.

The reasons for performing simulations of friction models are stated below:

I. Validation of friction models.

The behavior of the friction models must be investigated in some typical scenarios as a preliminary assessment. Through simulation, the performance of friction models

regarding accuracy, efficiency, and stability can be evaluated. In general, the accuracy can be evaluated by observing the simulated dynamic response and comparing it to the relevant experimental results, if available. The efficiency of the models can be evaluated from the computer time spent upon simulation. In the following sections, the properties of the different models discussed in this thesis are illustrated with simulation results.

II. Design of control system.

In high-precision servo mechanical systems, uncompensated friction is the major cause of performance degradation. Friction in mechanisms with adequate lubrication usually remains constant or varies slowly, and depends largely on the hardware configuration, e.g., the structure of motors and the layout of transmissions.

If a simulator of the hardware configuration is available, the simulation results can be studied for the corresponding mechanical system. From the results, it is possible to develop model-based compensation techniques where the direction and magnitude of friction can be predicted approximately. In the control system, an additional feedforward term can be added in the control law to compensate for the predictable part of friction. Thus the effects associated with friction can be eliminated or significantly reduced, and smooth motion for the mechanism can be achieved.

The simulation is important for evaluating various control strategies and testing the control gains.

III. Parameter identification.

In the identification schemes for friction parameters discussed in this thesis, the simulated response produced by the friction models with estimated friction parameters is compared to the actual experimental results, i.e., the objective function of the

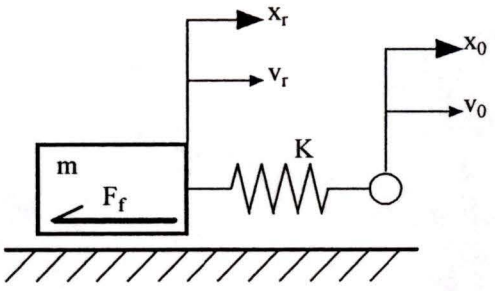

Figure 3.1: Simple Mass-Spring Example

identification problem is defined as the disparity between simulated response and the experimental results.

The simulations of different friction models were implemented in MATLAB® version 5.3.0 workplace under Windows NT® 4.0 operation system on Intel Pentium II® workstation running at 400 MHz. The software environment and hardware configuration were chosen because of their availability and flexibility. MATLAB® is a powerful matrix computational tool and it comes with an ODE solver, which has variable step-size integration [20].

3.1 Simple Mass-Spring System

3.1.1 Definition of the System Dynamics

A simple mass-spring model is used to simulate different friction models. The physical configuration was first introduced by Karnopp [13]. As shown in Figure 3.1, a mass-spring system is driven by the input velocity v_0 at point x_0. The spring K linking x_0 and mass m at x_r with deformation $(x_r - x_0)$ will apply a pulling force, or a possibly resisting force, on the mass m. The surface supporting mass m is a rough surface, and

friction force will be generated when mass m moves along it. It is assumed that under the effects of spring force and friction force, the mass m will demonstrate stick-slip phenomenon in its motion.

For numerical simulation, the motion of the system is defined by the following dynamics equations:

$$\begin{aligned} \frac{dx_0}{dt} &= v_0, \\ \frac{dx_r}{dt} &= v_r, \\ \frac{dv_r}{dt} &= \frac{1}{m}[K(x_0 - x_r) - F_f]. \end{aligned} \tag{3.1}$$

In (3.1) the friction force F_f will take different forms depending on different friction models as introduced in Chapter 2. The velocity v_0 is the only input to the system, and its value can be set to match certain situations, e.g., high speed or low speed motions. In the present simulation, v_0 is defined as

$$v_0 = 0.002, \text{ if } t > 0,$$

i.e., v_0 has a step change at $t = 0$ from zero to $0.002m/s$, a value in a low velocity range. The other physical parameter values of the system are defined as follows:

$$\begin{aligned} m &= 0.1kg, \\ K &= 100N/m. \end{aligned}$$

In this example, the normal contact force at the mass-surface interface is equal to the weight of the mass, which is just below $1N$. Considering a typical metal surface with a coefficient of kinetic friction of 0.2 to 0.3, we will assume a nominal sliding friction force of $0.2N$ and a peak stiction friction of $0.25N$. Note that in more general contact situations, such as robotic peg-hole insertion task, the normal contact force

is not constant but varies with the force applied by the robot to the payload from one moment to the next.

The particular physical setup of the example used here is not available for this thesis project and no experimental results can be presented. In some references, it is reported that stick-slip motion of the mass m can be observed in physical experiments [11] [1]. This phenomena can be regenerated from numerical simulation. When a valid friction model is implemented with appropriate parameters, the time-variant friction generated by the friction model may cause the mass to move in a stick-slip way, as we will see in the following numerical simulations. The reason for stick-slip motion is that the magnitude of friction is larger at rest than that during motion as described in §1.2.3. In the following simulations, all the friction models have been parameterized in order to generate stick-slip phenomenon.

Our way to gain some confidence in the simulated results is by checking the energy balance of the system. In particular, the following relationship must be true for the spring-mass example considered here:

$$E_i = E_s + E_k + W,$$

where E_i stands for the input energy to the system, W is the work done by friction force, E_s is the strain energy, and E_k is the kinetic energy.

The energy check is implemented by using the following error equation:

$$\varepsilon_{energy} = \left| \frac{E_i - E_s - E_k - W}{E_p} \right| \times 100\% \tag{3.2}$$

where E_p denotes the peak energy level. The calculation methods for the energy and work variables are listed as follows. The strain energy of the spring K can be

calculated as

$$E_s = \frac{1}{2}K(x_0 - x_r)^2$$

and the kinetic energy of the mass m can be calculated as

$$E_k = \frac{1}{2}mv_r^2$$

The energy input E_i to the system is the work down by the external force at the point x_0, and can be evaluated from

$$E_i = \int (F_{spring} v_0) dt,$$

where F_{spring} is the spring force and v_0 is the input velocity at the point x_0.

The function (3.2) gives the percentage error of the maximum energy during the motion. The energy balance error is calculated at each time instant during the simulation time span. The energy error for different friction models is plotted together with the simulated response of motion and friction force.

3.1.2 Simulation of Classical Model

The formulation and characteristics of the Classical Model were presented in §2.2.1. The parameters used in the present simulation are listed as follows:

$$\begin{aligned} v_1 &= 1 \times 10^{-4} m/s \\ v_2 &= 2 \times 10^{-4} m/s \\ F_1 &= 0.2N \\ F_2 &= 0.25N \end{aligned}$$

The values of v_1 and v_2 are set very small to be located in the low velocity region.

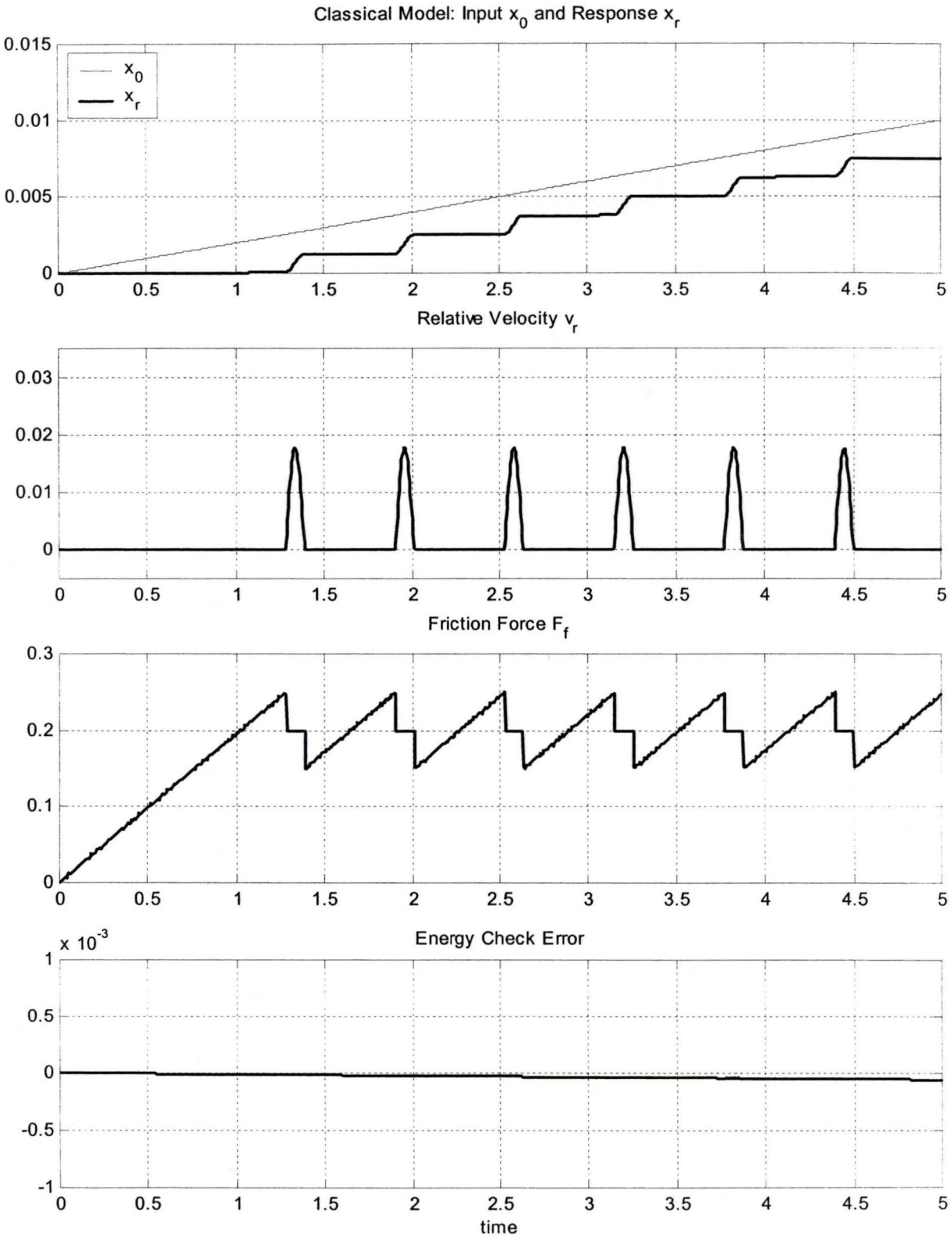

Figure 3.2: Simulation Results from Classical Model on Mass-Spring System

The simulation yields the results for state variables including the displacement and velocity of the mass m, and the contact friction F_f, which are plotted respectively in Figure 3.2. From the displacement plot, we can see that the mass m is initially at rest, and from $t = 0$ to $t = 1.25s$, the applied force caused by deformation of spring increases linearly with x_0:

$$F = K(x_0 - x_r).$$

During this short period of time, the mass m remains at rest, i.e., $x_r \simeq 0$, which can be explained by the fact that the friction force from the surface to the mass counteracts the spring force.

The mass m is kept from moving until $t = 1.25s$, when the maximum friction force is reached and exceeded by the spring force. After $t = 1.25s$, the mass slides under the combined effect of the spring force and the friction force, moving in a typical "stick-slip" fashion. From the subplot of relative velocity, the changes of velocity in stick-slip can be observed. From a zoomed view of the plot of x_r, it can be seen that the values of x_r before $t = 1.25s$ are not exactly zero but approximately $7 \times 10^{-5}m$. This is the so-called presliding displacement, which is one of the non-linear characteristics discussed in §1.2.3.

As discussed before, the most important characteristics of the Classical model are the slopes of $\frac{F_1}{v_1}$ in $[0,\ v_1]$ and $\frac{F_1 - F_2}{v_1 - v_2}$ in $[v_1,\ v_2]$, which in turn make the velocity-friction relation continuous for very slow motion. According to the formulation of the Classical model, it requires a low level of velocity to generate the stiction when $|v_r| < v_1$. The integration of the slight velocity is the presliding displacement in this model.

One problem with this model is its numerical conditioning, in particular, its sensi-

tivity to values of v_1 and v_2. It they are chosen too close, it may be difficult to calculate the slope $\frac{F_1 - F_2}{v_1 - v_2}$ as this may cause a "divide by zero" error during simulation on some computer systems.

3.1.3 Simulation of Karnopp Model

The Karnopp model is a 3-parameter model as described in §2.2.2. The parameters used in the simulation are:

$$\begin{aligned} F_H &= 0.25N \\ F_{slip} &= 0.20N \\ D_v &= 2 \times 10^{-4} m/s \end{aligned}$$

The value of the velocity bound D_v must be set very small in the low velocity regime, similar to the critical velocities v_1 and v_2 in the Classical model. The simulation results for the simple mass-spring system obtained with the Karnopp model are shown in Figure **??**. As shown in the plot, in the first stiction period from $t = 0$ to $1.25s$ the friction force generated between the contact surface cancels out the applied spring force; thus the mass remains at rest with exact zero displacement, zero velocity, and zero acceleration.

At $t = 1.25s$, the spring force reaches the maximum static friction F_H and the mass m begins to slide and then proceeds in a stick-slip fashion under the combination of the spring force and the friction force. From the plots of friction force we can see that it is increasing smoothly during pre-sliding stages, and has a step change from maximum stick friction to the lower sliding friction.

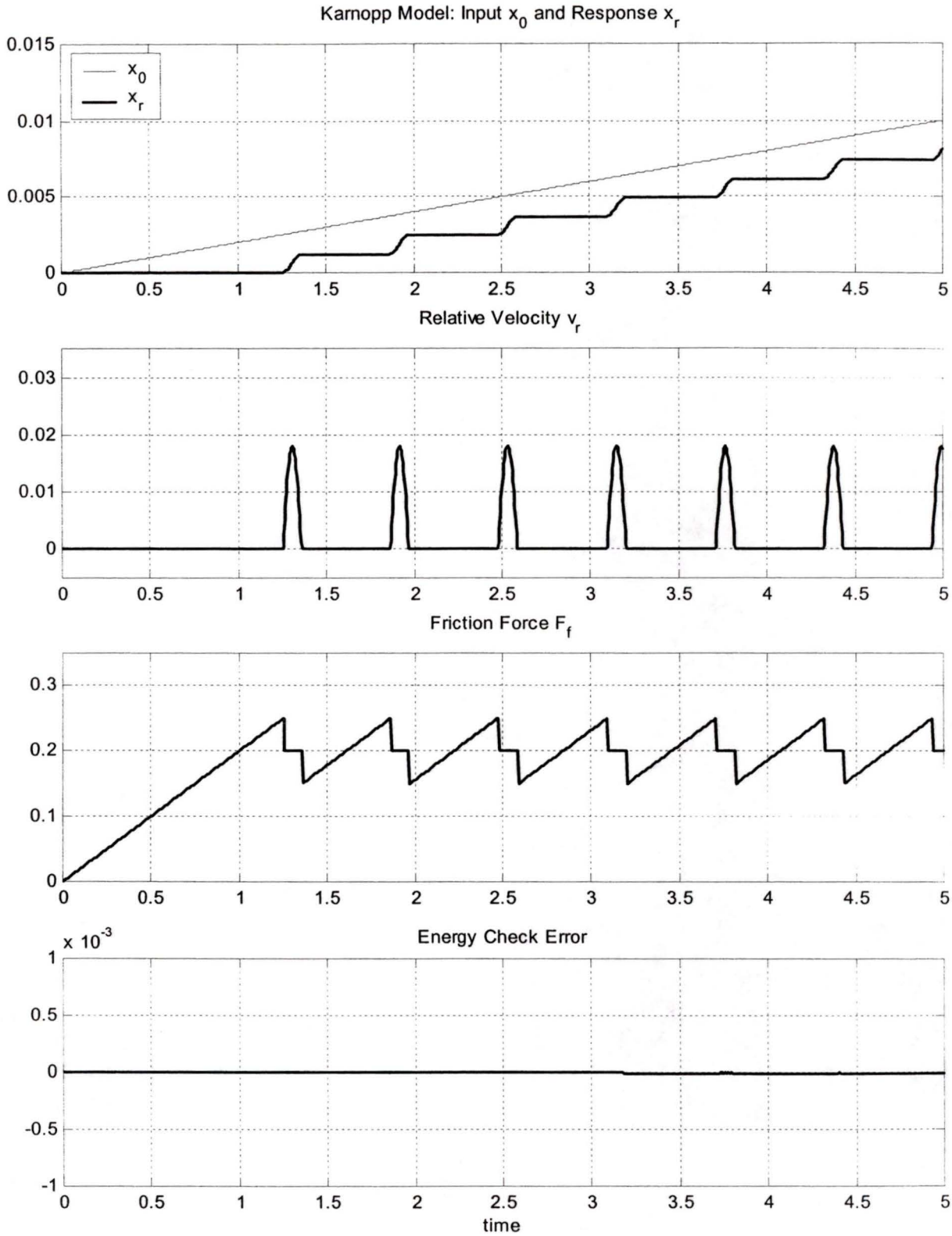

Figure 3.3: Simulation Results from Karnopp Model on Mass-Spring System

In the Karnopp model, when the velocity is smaller than the velocity bound, i.e.,

$$|v_r| < D_v,$$

the applied forces will be cancelled out by the Karnopp static friction force until the applied outside force increases to the level that exceeds the maximum static friction force F_H. While the sum of the forces is zero, there is no acceleration, no velocity and no displacement between the two contacting surfaces. No presliding displacement is included in this model.

The simulation of the Karnopp friction model is significantly faster compared to the other models. The reason for this is that its formulation is simpler than other friction models and requires less arithmetic and logic evaluations. The drawback of the Karnopp model is that it requires an input of the observed applied force, e.g., the spring force in the simple mass-spring example. In this case, the spring force applied to the mass can be estimated by the deflection of the spring multiplied by the stiffness of the spring, which is known. But in a more practical system this kind of applied force is not always observable.

The parameters in the Karnopp model are not equivalent to the parameters in the above-mentioned Classical model during simulation. Their simulation results are slightly different. In the Karnopp model, the stiction does not do any work during sticking as there is no displacement, but in the Classical model stiction is a working force as there is a slight presliding displacement. The final displacements of these two models at $t = 5$ are not the same. Their values are listed in Table 3.2 together with simulation results from the other friction models.

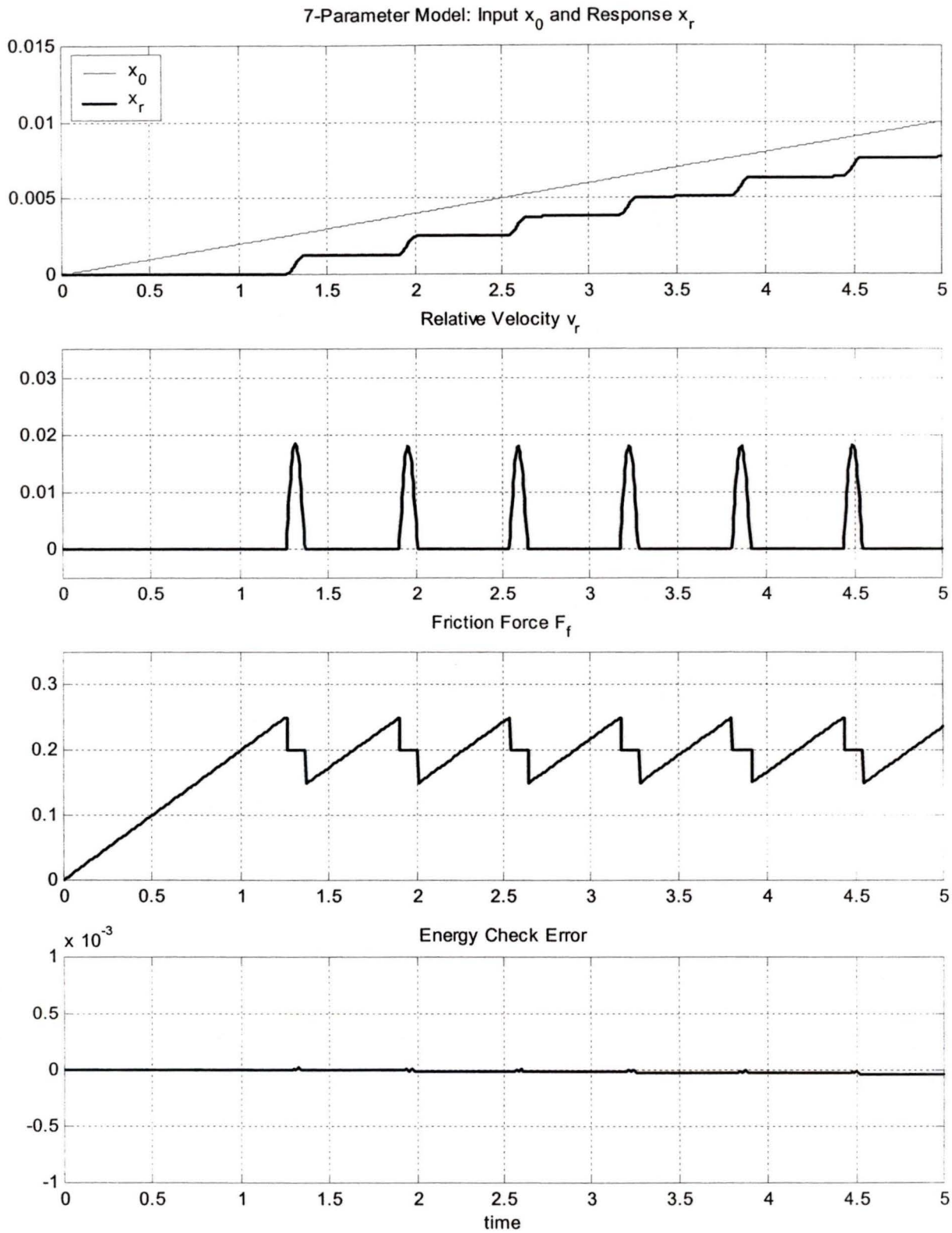

Figure 3.4: Simulation Results from 7-parameter Model on Mass-Spring System

3.1.4 Simulation of 7-parameter Model

The original formulation of the seven-parameter model was introduced in §2.2.3. To implement this model in a computer, the model has to be slightly modified as suggested in [15]. A velocity bound D_v needs to be included to define the sticking stage. The parameter τ_L and the corresponding term in the model are dropped for computing efficiency. The parameters used in the simulation are listed as follows:

$$\begin{aligned} F_c &= 0.2N \\ F_v &= 0.01N \\ F_{s,\infty} &= 0.25N \\ k_t &= 1 \times 10^4 N/m \\ \dot{x}_s &= 0.0001m/s \\ \gamma &= 100s \\ D_v &= 1 \times 10^{-4} m/s \end{aligned}$$

The simulation results are shown in Figure 3.4. In this model, the stiction and kinetic friction levels are defined with $F_{s,\infty}$ and F_c respectively. The simulated friction response of the 7-parameter model is sensitive to these two major parameters. Because the example used here is in the low velocity regime, the velocity-dependent features of friction are not significant.

3.1.5 Simulation of Bristle Model

The formulation of the Bristle model was introduced in §2.3.1. The implementation of the Bristle model in a numerical simulator is somewhat subtle, as a random number generator is needed to calculate the bristle positions which must be "uniformly

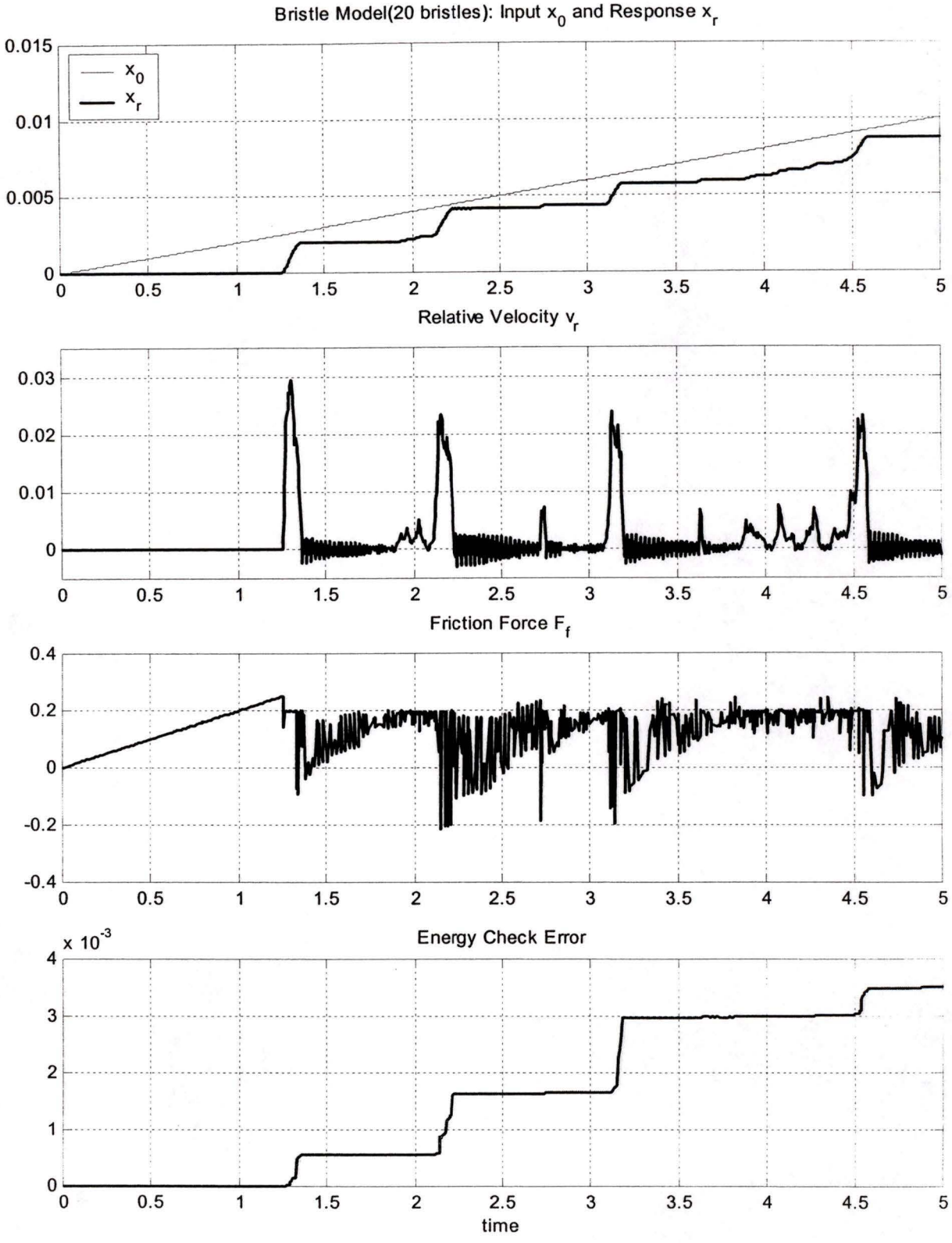

Figure 3.5: Simulation Results from Bristle Model on Mass-Spring Example

distributed" over the contact surfaces. The parameters used in this simulation are as follows:

$$\begin{aligned} \delta_s &= 1 \times 10^{-5} m \\ k_b &= 1250 N/m \\ N &= \begin{cases} 20, \text{ when sliding} \\ 25, \text{ when sticking} \end{cases} \\ \Delta &= 0.8 \times 10^{-5} m \end{aligned}$$

and the simulation results are shown in Figure 3.5. From the third plot we can see that the friction force is quite noisy or "hashy". The roughness of the friction values comes from the randomly generated bristle positions. As a result of this, energy balance is not very well maintained with this model. The energy balance error decreases for smaller integration step size and the details of the response also change somewhat.

3.1.6 Simulation of Reset Integrator Model

The Reset Integrator model is an alternative version of the Bristle model, and it considers the aggregate behavior of multiple bristles as introduced in §2.3.3. It is a better formulation as it uses a single bristle variable to represent the statistical response of multiple bristles. The parameter set used in our simulation is as follows:

$$\begin{aligned} p_0 &= 10^{-5} m \\ k_r &= 2 \times 10^4 N/m \\ a &= 0.25 \\ \beta &= 30 Ns/m \end{aligned}$$

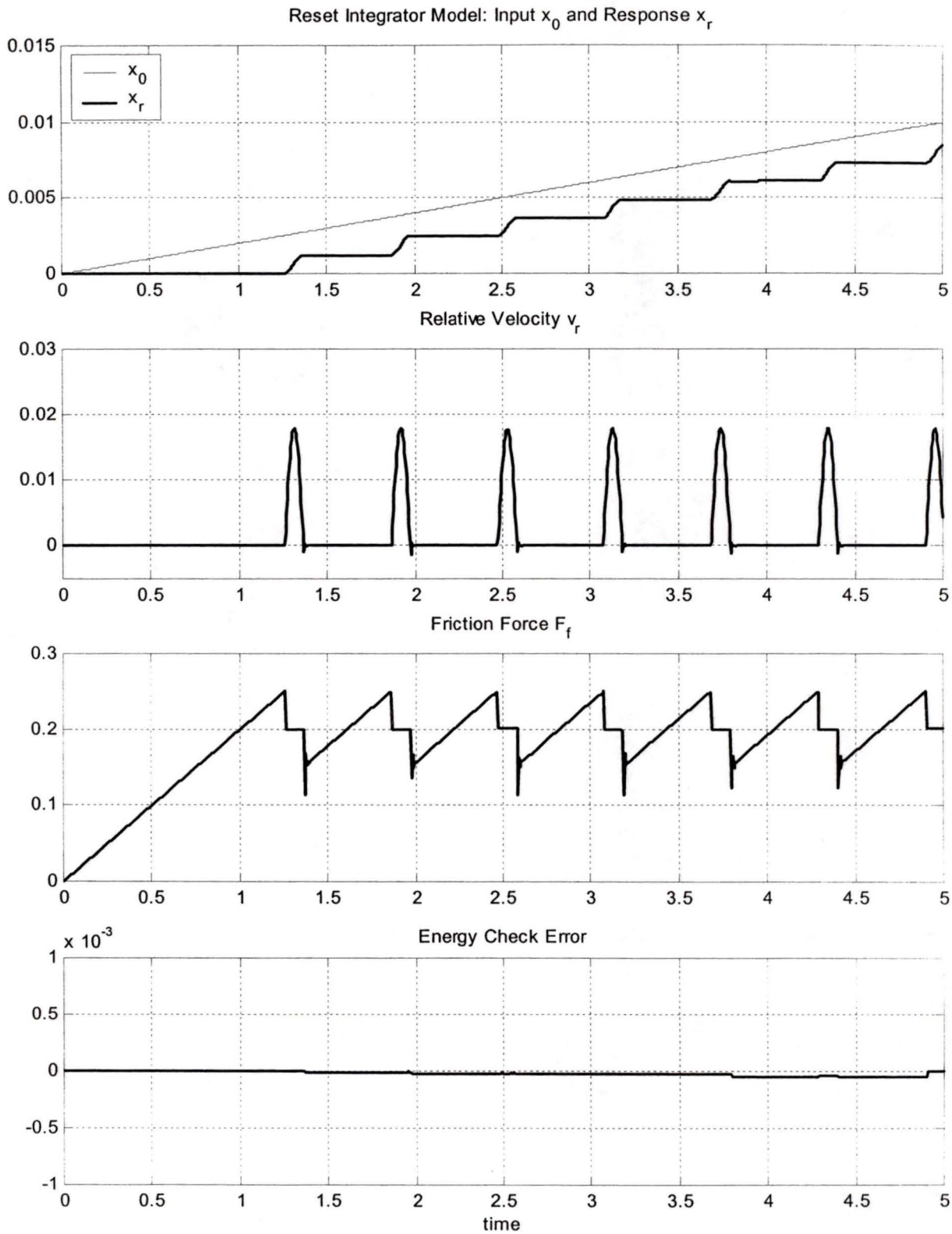

Figure 3.6: Simulation Results from Reset Integrator Model on Mass-Spring System

These values were chosen after several test runs attempting to ensure that the dynamic response is similar to those generated in the Classical model and the Karnopp model. The parameters will drive the model to generate a sliding friction at $0.2N$ and a maximum stiction friction of $0.25N$.

The simulation results are shown in Figure 3.6 and demonstrate similar dynamic performance to the traditional static friction models, including the Classical model and the Karnopp model.

3.1.7 Simulation of LuGre Model

The LuGre model was proposed by Canudas de Wit *et al.* in [7]. The parameters used in this simulation were chosen as listed below:

$$\begin{aligned} v_S &= 0.001 m/s \\ \sigma_0 &= 10^5 N/m \\ \sigma_1 &= \sqrt{10^5} Ns/m \\ \sigma_2 &= 0.4 \\ F_C &= 0.2N \\ F_s &= 0.25N \end{aligned}$$

The simulation results are shown in Figure 3.7.

The LuGre model was implemented and simulated with the parameters chosen to produce a response comparable to the other models. However, the LuGre model is very complicated, as it was designed to include many features of friction. In the present simple example, the dynamic responses for velocity and displacement of the LuGre model with the chosen parameter set are similar to those of the other models.

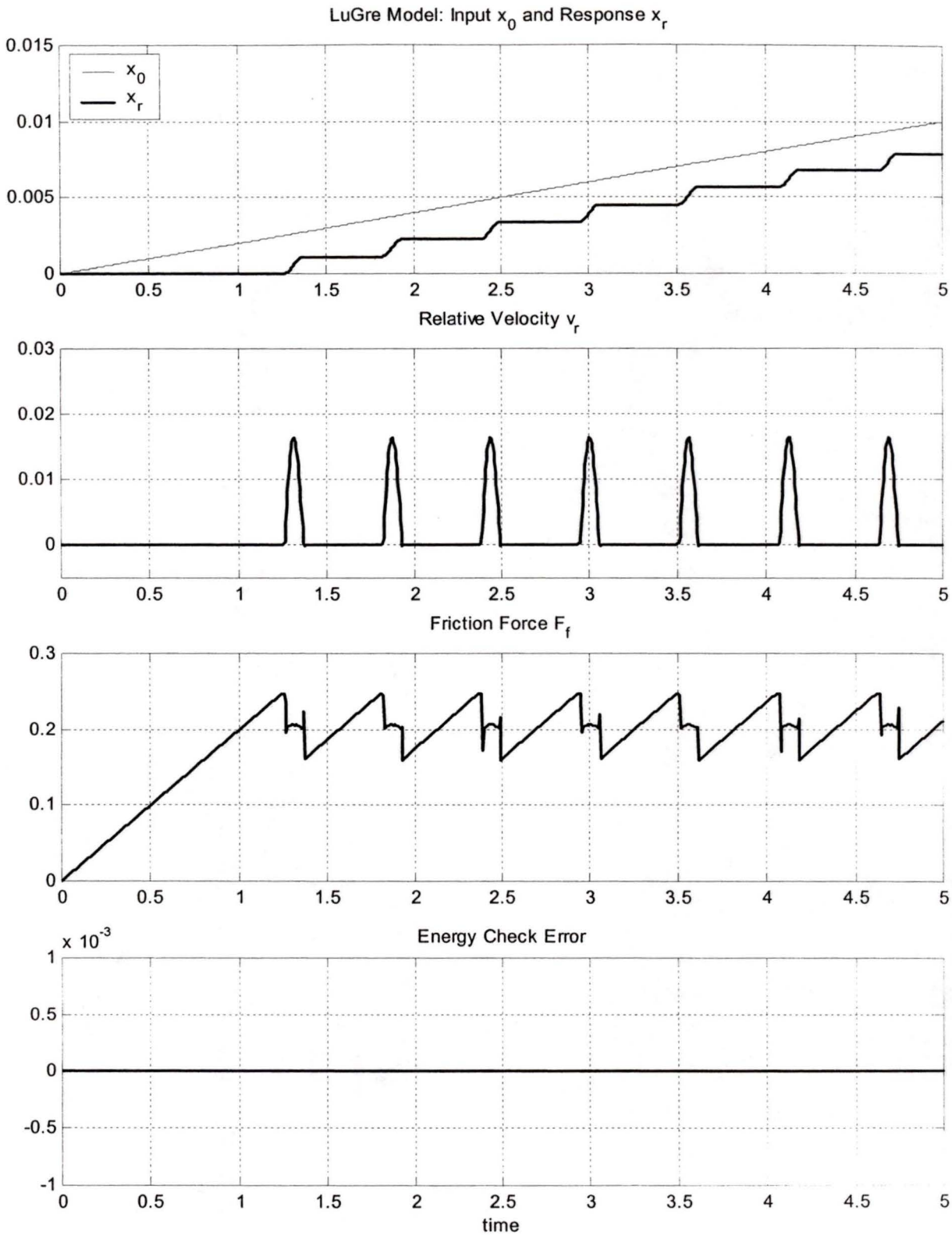

Figure 3.7: Simulation Results from LuGre Model on Mass-Spring System

However, the friction force profile of the LuGre model is more complex than those of other models. In the LuGre model, the parameters of F_s and F_C define the stiction and kinetic friction, so the simulated response of friction is sensitive to these two parameters. The other parameters will only slightly influence the simulated friction when the relative velocity remains constant or varies slowly. A master's thesis was completed by Gäfvert in [10], where the author carried out extensive research on this model including its formulation, linearization, and identification. More details on the LuGre model can be found in that work.

3.2 Mass-Spring System with Multiple-Point Contacts

In this section, we present simulation results for a more complicated system consisting of two masses and two springs. The schematic of this example is shown in Figure 3.8. An important distinguishing feature of this example is that the second mass m_2 is in two-point contact: it is in contact with the ground and itself is supporting the first mass m_1 on its upper surface. This example allows us to evaluate the ability of different friction models to deal with multiple-contact-point situation.

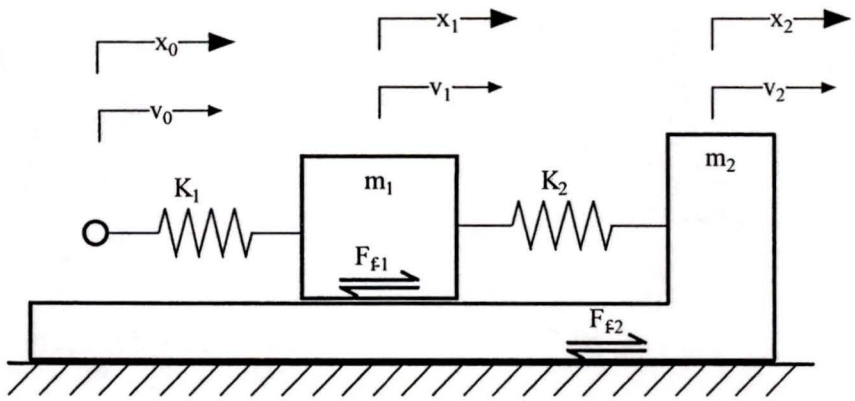

Figure 3.8: Two-mass-spring System

The system parameters are listed as follows:

$$
\begin{aligned}
m_1 &= 0.1kg, \\
m_2 &= 0.1kg, \\
K_1 &= 100N/m, \\
K_2 &= 200N/m.
\end{aligned}
$$

The input velocity v_0 has a step change at $t = 0$ from zero to $0.2m/s$ and returns to zero at $t = 0.25s$. The friction force between the mass m_1 and m_2 is denoted as F_{f-1}, while F_{f-2} denotes the friction force between m_2 and the ground.

The Classical model, Karnopp model, Bristle model and Reset Integrator model are implemented for this example. The parameters used in these friction models are listed in Table 3.1. The parameters are chosen to generate an average kinematic friction force of $0.1N$ and $0.2N$ and peak stiction levels of $0.15N$ and $0.3N$ for F_{f-1} and F_{f-2}.

The simulated responses for different models are shown in Figure 3.9. From the plots of the simulated responses with different friction models, the values of relative velocity are matchable, while the values of friction force exhibit significant difference. This is due to the fact that the internal dynamics of these friction models are different. As a result, they don't follow the same way of increasing or decreasing their friction levels.

Table 3.1: Friction Model Parameters for Two Body Example

Model	Parameters	F_{f-1}	F_{f-2}	Units
Classical Model	v_1	1×10^{-4}	1×10^{-4}	m/s
	v_2	2×10^{-4}	2×10^{-4}	m/s
	F_1	0.15	0.3	N
	F_2	0.10	0.2	N
Karnopp Model	D_v	10^{-4}	10^{-4}	m/s
	F_H	0.15	0.3	N
	F_{slip}	0.10	0.2	N
Bristle Model	δ_s	10^{-5}	10^{-5}	m
	k_b	1.5×10^4	1.5×10^4	N/m
	N	1	1	
	Δ	0.33×10^{-5}	0.33×10^{-5}	m
Reset Integrator Model	p_0	10^{-5}	10^{-5}	m
	k_r	1×10^{-4}	2×10^{-4}	N/m
	β	40	40	Ns/m
	a	0.5	0.5	

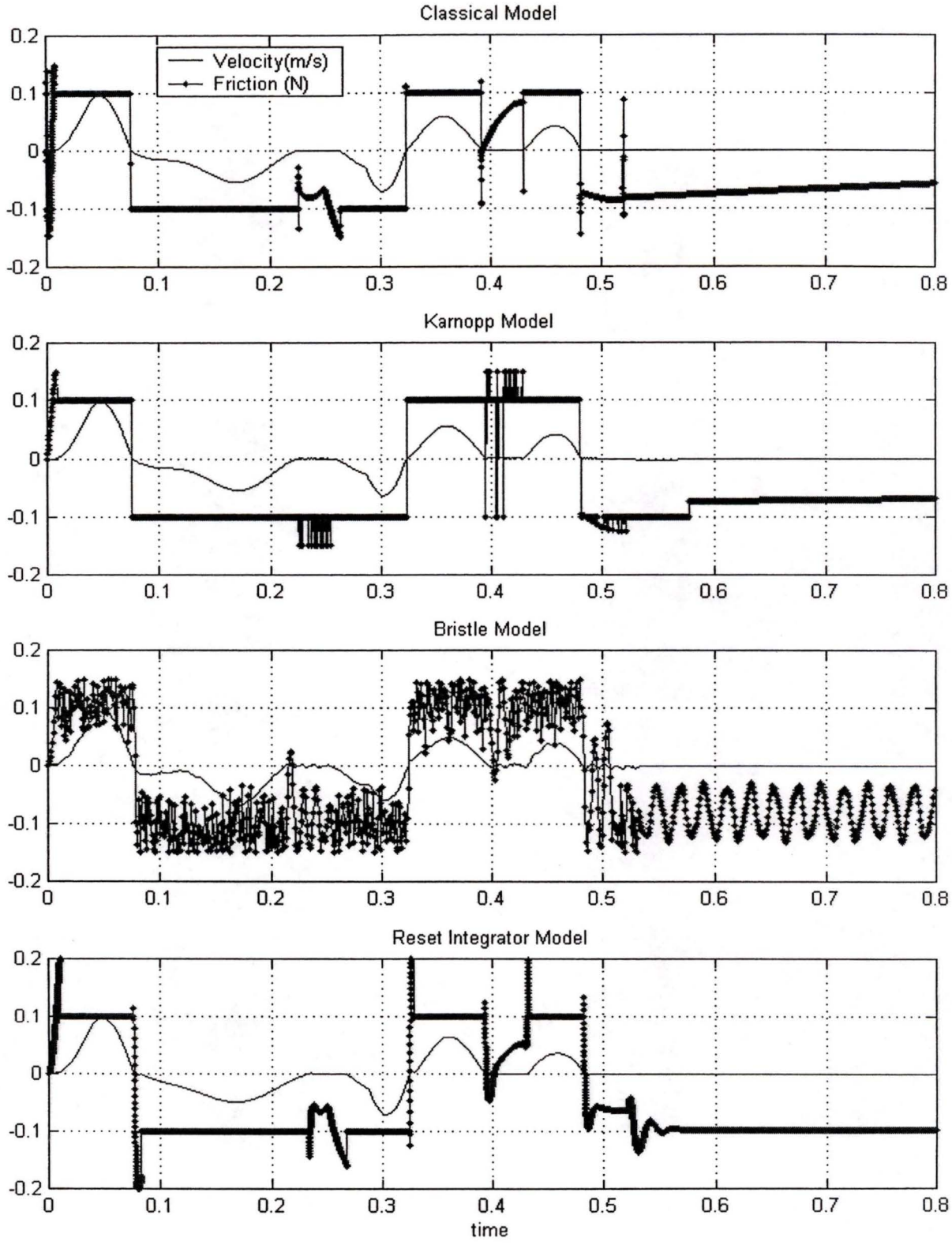

Figure 3.9: Simulated Relative Velocity and Frcition between m_1 and m_2

Table 3.2: Comparison of Simulated Displacement Values and Energy Error at t=5s for Simple Mass-Spring System

Model	x_r	ε_{energy}
Classical Model	7.52×10^{-3}	0.006%
Karnopp Model	7.53×10^{-3}	0.0001%
Bristle Model	7.89×10^{-3}	0.3%
Reset Integrator Model	8.49×10^{-3}	0.005%
7-Parameter Model	7.64×10^{-3}	0.003%
LuGre Model	7.89×10^{-3}	0.0005%

3.3 Discussion of Results

From the simulation responses, it is difficult to evaluate the accuracy of different friction models without experimental data. In the simple mass-spring case, simulation results can at least be used to make a qualitative assessment of the model performance as well as to compare the various models with each other. The relative motions of the mass and the base x_r caused by all the models except the Bristle model are almost identical. The displacements of the mass at the end of the numerical simulation calculated for different friction models are listed in Table 3.2. Also listed are the energy errors for different friction models, and we can see that for all friction models except the Bristle model the energy balance is very well maintained.

The computational times for each model's simulation of the mass-spring example considered in this chapter are presented in Table 3.3. This table indicates that there is a substantial difference in the computational efficiency of the different models.

Table 3.3: Computer Time Comparison

Model	**Elapsed Time (s)**	
	One-body Example	Two-body Example
Classical Model	195.29	63.74
Karnopp Model	3.25	6.29
Bristle Model	218.67	89.56
Reset Integrator Model	6.13	24.25
7-Parameter Model	154.21	N/A
LuGre Model	12.36	N/A

The simulated results for all friction models predict the occurrence of significant stick-slip motion. This implies that all models are capable of predicting some of the non-linear features of real friction force at low velocities, even under the multiple-point-contact situation.

Additional simulations with higher input velocity v_0 were also conducted in the simple mass-spring example. It was noticed that in this case there is no stick-slip for the motion of mass m. This represents some proof that certain frictional features present at a low velocity would disappear at a higher velocity.

From all results, we conclude that the Karnopp, Reset Integrator, and LuGre models are appropriate choices for the simulation of dynamic processes where friction is a significant factor. In view of their dynamic performance and computational efficiency, these models can be used in real-time compensation schemes.

Chapter 4

Non-Linear Friction Parameter Identification

4.1 Background

The simplest aspect of friction parameter identification is to determine the friction coefficient μ in Coulomb model. In principle, for the case shown in Figure 4.1, when the mass is not accelerating, μ can be calculated as the ratio of the force required to maintain the motion over the normal contact force, i.e.,

$$\mu = \frac{F_f}{F_n}. \tag{4.1}$$

The above assumes that μ is independent of contact physics, for example, in this case the contact area between the mass and the surface. Empirical μ values for different materials have been measured in this way and listed in engineering handbooks [2] [22].

As discussed in previous chapters, friction is a more complex phenomenon than

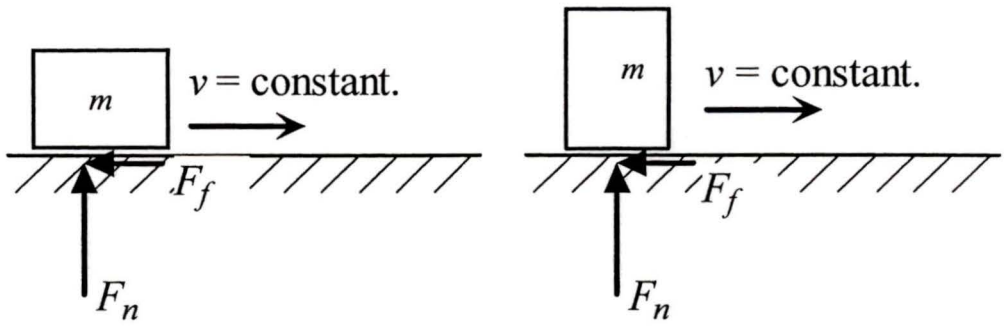

Figure 4.1: Calculation of μ for Coulomb Friction

what is captured by the Coulomb model, but contains many non-linear characteristics, including stiction, Stribeck effect, stick-slip, velocity dependence and input frequency dependence. However, for the recent non-linear friction models developed, the parameter identification becomes difficult since parameters of these models cannot be directly acquired from the traditional measurements, one after another.

In tribology, a synthesized approach is formulated to compute friction coefficient μ and other contact parameters. The frictional parameters are retrieved from the material-dependent properties of contact surfaces, as well as circumstantial physical conditions including surface cleanliness, lubrication, temperature, and speed of relative motion [3].

For mathematical friction models such as those presented in the previous chapters in this thesis, it is advisable to use a numerical identification procedure to process the experimental data and extract the desired friction model parameters. If the identified parameters are valid, they must be able to provide a simulated response, which is dynamically matchable to the experimental response. In the literature, there are many works addressing the techniques for identification of friction forces or

friction parameters. Furthermore some of the researchers who proposed or modified friction models also suggest a parameter identification method for their models. This indicates that the parameter identification problem is an important aspect of research on friction.

In the recent literature, the trend has been to formulate the parameter identification problem as an optimization problem because of the non-linear characteristics of friction models [26]. In principle the effective analytical solution can not be found. Therefore non-linear numerical methods must be used to solve this kind of problem. The strategies, application, and conclusion on the numerical methods are discussed in detail in the papers reviewed below.

In 1988, a simple method for identification of Karnopp stick-slip friction using a numerical optimization approach was proposed by Cheok *et al.* [5]. The authors noted that multiple minima are possible and can be problematic for the gradient-based line search method. The *Modified Simplex Algorithm* was implemented to identify the system parameters in a servomotor system including slip and stick friction torques. The system parameters are identified by minimizing the mismatch between the plant and the model.

From 1996 to present, a series of papers addressing parameter identification of the 7-parameter model [1] were presented by Jeon *et al.* [12] and Lee *et al.* [15]. In these papers, evolution strategies and genetic algorithms are applied to their numerical identification methods. As described in [15], "*these algorithms are based on an arbitrarily initialized population of trial solutions, which by means of randomized process of selection, mutation, and recombination, evolves towards successively better regions in the search space.*"

In 1997, a general model-independent identifier with a Gaussian network was pro-

posed by Du *et al.* [8]. A compensation scheme using this identifier was implemented in a position controller. The stability and accuracy of the identifier was validated through the simulation of the control scheme.

There are many reasons for studying parameter identification for friction models. The typical application of friction identification is to control of mechanical systems, such as high-precision servo mechanisms and robotic manipulators. The importance of friction compensation was discussed in Chapter 2. The identified parameters would help in defining control gains for a traditional feedforward controller. Moreover effective on-line identification methods can be incorporated in the recent advanced control strategies such as adaptive control scheme [17].

In this thesis project, the major motivation is to identify the parameters of the Modified Bristle model used in MDSF to provide users of this facility with the required inputs for simulating constrained robotic operations.

4.2 Theory of Non-linear Parameter Identification

4.2.1 Formulation of the Problem

Defining the identification procedure for an unknown set of dynamic parameters is not trivial from either a theoretical or a practical point of view. The problem is posed as follows: for a non-linear friction model with a given structure, is it possible to determine the exact values of its parameters from the system responses which are partially effected by the model?

A simple parameter optimization problem may be stated as follows: determine the values of the ordered set of n parameters each representing an independent parameter in the friction model:

$$P = [p_1\ p_2,\ ...p_n], \tag{4.2}$$

which minimize the objective function

$$f_F(\hat{P}) = \left\| \hat{\mathbf{X}}_F - \mathbf{X}_F^{\text{exp}} \right\|, \tag{4.3}$$

where $\hat{P}$ denotes the estimation of parameter set P, $\mathbf{X}_F^{\text{exp}}$ is the vector of experimentally measured friction values, and

$$\hat{\mathbf{X}}_F = X_F(\hat{P}),$$

is a vector of simulated friction values calculated with the estimated parameter set $\hat{P}$, $X_F(\cdot)$ is the mapping function of the parameter set to the simulated friction response.

The objective function $f_F(\hat{P})$ is defined so as to evaluate the suitability of parameter estimates $\hat{P}$ by measuring the discrepancy between the simulated friction values and the experimental friction values. Note that there are some variations in the form of the objective function and they will be discussed in §4.2.3.

4.2.2 Optimization Based Identification Procedure

In general, an optimization-based algorithm to solve the parameter identification problem contains the following steps:

Step I. Set the tolerance ε as a very small number, e.g., $\varepsilon = 10^{-6}$; set iteration counter $k = 0$; define initial configuration, i.e., the initial parameter set

$$\hat{P}^0 = [\hat{p}_1^0,\ \hat{p}_2^0,\ ...\hat{p}_n^0]. \tag{4.4}$$

Step II. Simulate the dynamics of the system to get $\hat{\mathbf{X}}_F^k = X_F(\hat{P}^k)$.

The estimated parameter set $\hat{P}^k$ is used as input to the friction model in the simulation. The output simulated response is $\hat{\mathbf{X}}_F^k$, which contains the values of state variables for all the time steps stacked as a vector.

Step III. If $f(\hat{P}^k) = \left\|\hat{\mathbf{X}}_F^k - \mathbf{X}_F^{\exp}\right\| > \varepsilon$, continue with Step IV; otherwise if $f(\hat{P}^k) \leqslant \varepsilon$, terminate the procedure and output $P = \hat{P}^k$.

The objective function $f(\hat{P}^k)$ is defined as the discrepancy between the simulated response $\hat{\mathbf{X}}_F^k$ and the experimental response $\mathbf{X}_F^{\exp}$. After a finite number of iterations, $\hat{P}^k$ becomes the current parameter set, if the objective function value $f(\hat{P}^k)$ is smaller than the tolerance ε, then $\hat{P}^k$ is declared as the final parameter estimate of the identification procedure.

The number of maximum iterations is set to k_{max} to confine the time spent on calculation.

Step IV. With a gradient-based method, update the parameter set to $\hat{P}^{k+1} = [\hat{p}_1^{k+1},\ \hat{p}_2^{k+1}...\hat{p}_n^{k+1}]$, set $k = k + 1$, and return to Step II.

In this step, one uses a gradient-based method or any other numerical optimization technique to calculate a new parameter set $\hat{P}^{k+1}$ to start the next iteration.

4.2.3 Alternative Objective Functions

There are several methods to evaluate the quality of the estimated parameters, or to define the objective function. Each method has its advantages and drawbacks in terms of feasibility and efficiency. In general, the objective function takes the form of the difference between the simulated system response with estimated parameters and respective experimental values. For example, when the estimated parameter set $\hat{P}$ is substituted into the friction model used in simulation, the values of state variables can be calculated and compared to the respective measurements, such as displacements, velocities, and contact friction force which are collected during a practical test.

It was mentioned above that the objective function for friction parameter identification takes the form of (4.3), where the simulated and experimental friction values were compared. However, friction sensors are still in development stage and have not been widely used [25]. As well, it is at least impractical, if not impossible, to implement friction sensors into a general contact interface. Therefore, it is not the usual case to measure the friction forces directly in normal experiments. However, if friction values can be somehow extracted from other experimental data, then the friction measurements can be separated and used to determine the parameters of arbitrary friction models. An example of this approach, the peg-hole insertion case, will be presented in Chapter 5.

Alternatively, when the motion response of the system is available in the experimental data, it is ideal to compare the simulated motion, including displacements

and/or velocities, to the experimental measurements of motion. Thus the motion-measurement objective function of optimization is formulated in the form:

$$f_X(\hat{P}) = \left\| \mathbf{X}(\hat{P}) - \mathbf{X}^{\text{exp}} \right\|, \tag{4.5}$$

where

$$\begin{aligned} \mathbf{X}(\hat{P}) &= \text{ simulated motion with } \hat{P}, \\ \mathbf{X}^{\text{exp}} &= \text{ experimental motion.} \end{aligned} \tag{4.6}$$

Let us assume a practical parameter identification case involved with friction: a physical apparatus equipped with displacement sensors, which will measure the motion response during an experimental test. We will also assume that the kinetic model of the system is known and is based on a particular friction model whose parameters are to be identified. Furthermore, a given set of friction parameters P will ensure a unique simulated response $\mathbf{X}(P)$. If a critical parameter set $\hat{P}$ can be found to provide a particular simulated response of displacement $\mathbf{X}(\hat{P})$, which is identical to the experimental response of displacement $\mathbf{X}^{\text{exp}}$, i.e., $f_X(\hat{P}) = \left\| \mathbf{X}(\hat{P}) - \mathbf{X}^{\text{exp}} \right\| \approx 0$, this means that $\hat{P}$ is the ideal parameter set for the friction model in this case.

A numerical evaluation of the performance of different optimization procedures provides an initial step towards solving the identification problem. In this case, the simulated response of a friction model with "correct" parameters is used as an alternative to the experimental data. The simulated responses with estimated parameters are compared to the exact simulation with "correct" parameters in the objective function.

In the next section, the simple mass-spring case presented in Chapter 3 is used as an example to evaluate numerically the validity of identification procedures. For this example, the motion simulator is defined as $X(P)$, and the simulated response

of displacement is employed in the objective function in the form

$$f(\hat{P}) = \left\| \mathbf{X}(\hat{P}) - \mathbf{X}(P^{\text{correct}}) \right\|, \tag{4.7}$$

where $\mathbf{X}(\bullet)$ is the mapping function from parameter set to motion response and

$$\begin{aligned} \mathbf{X}(\hat{P}) = &\quad \text{simulated displacement with parameter set } \hat{P}, \\ \mathbf{X}(P^{\text{correct}}) = &\quad \text{simulated displacement with parameter set } P^{\text{correct}}. \end{aligned} \tag{4.8}$$

It has not been rigorously proven but generally accepted that there exists a global minimizer for the objective function (4.7), as shown in the following mass-spring example. The reason is that the mapping function is unique, so only when $\hat{P} = P^{\text{correct}}$, $\mathbf{X}(\hat{P}) = \mathbf{X}(P^{\text{correct}})$. As a result, P^{correct} can be found by means of gradient-based line search method. For objective functions like (4.3) and (4.5), as practical physical system is involved, there may exist a global minimizer if the numerical model of mapping the parameter set to the system response is unique.

4.2.4 Multiple Initial Configurations

The initial estimate for the parameter set $\hat{P}^0$ in (4.4) can be either arbitrarily defined or created by a random number generator in the parameter space. It has been noted that the optimization results calculated with different initial values are not always the same when a general gradient-based line search scheme is used. According to the analysis by Du *et al.* [8], the pure gradient method is not suitable for the above-mentioned parameter identification problem because of the following reasons:

1) an explicit closed-form gradient expression for the non-linear system model response can not be found;

2) the objective function is generally not convex over the parameter space, i.e., multiple minimizers may exist for the minimization problem;

3) the objective function varies very slowly with the changes of some parameters under certain system excitation conditions.

Based on the idea of *Genetic Optimization*, multiple initial configurations are proposed and utilized to cover the diversity of the parameter search space. By employing more than one initial configuration, we are more likely to find the parameter set which will provide the best fit to the measured experimental data, since there is no guarantee that the objective function is convex and a particular initial parameter set will produce convergence towards the global minimizer, or the optimal parameter set, with a line search algorithm.

Based on the simulation tests with the simple mass-spring system, it was found that the initial sample of 20 randomly chosen sets in the parameter space is diverse enough to ensure satisfactory parameter estimation. The final optimum parameter set chosen among the 20 results from different initial sets is nearly identical to the "correct" parameters.

4.3 Identification for the Mass-Spring Numerical Example

The implementation of friction models for the simple mass-spring example and the corresponding simulation results were discussed in Chapter 3. During simulation with the "correct" parameters, the state variables, including displacement, relative velocity, and friction force, are calculated as a function of time and stored in an array. These

values are defined as the *original* simulation results. Then, the displacements are utilized in the objective function defined in equation (4.7). The procedure proposed in §4.2.2 is utilized to solve the optimization problem of finding the optimal parameter set which minimizes

$$f(\hat{P}) = \left\| \mathbf{X}(\hat{P}) - \mathbf{X}(P^{\text{correct}}) \right\|.$$

The above optimization problem was solved with a function from Optimization Toolbox® of MATLAB®.

4.3.1 Identification of Classical Model Parameters

Standard Formulation

For identification of Classical Model parameters, the optimization problem was formulated as follows: minimize the objective function

$$f_c(\hat{P}_c) = \left\| \mathbf{X}(\hat{P}_c) - \mathbf{X}(P_c^{\text{correct}}) \right\| \tag{4.9}$$

of the 4-parameter set $\hat{P}_c = [\ \hat{v}_1 \quad \hat{v}_2 \quad \hat{F}_1 \quad \hat{F}_2\ ]$, with constraints

$$\begin{aligned} v_2 &> v_1 > 0, \\ F_1 &> F_2 > 0. \end{aligned} \tag{4.10}$$

As discussed before, P_c^{correct} is the parameter set used in the simulation, and the simulated response with P_c^{correct} was presented in §3.1, where

$$P_c^{\text{correct}} = [1 \times 10^{-4} \quad 2 \times 10^{-4} \quad 0.25 \quad 0.20]. \tag{4.11}$$

As noted before, different initial conditions do not always result in convergence to the correct parameter values. By using multiple initial conditions, as discussed in §4.2.4,

20 optimal parameter sets were produced from 20 random initial conditions. Finally the best solution, as measured by the value of the objective function, is obtained from the initial condition defined by the following parameter set:

$$\hat{P}_c^0 = \begin{bmatrix} 2.722 \times 10^{-4} & 8.214 \times 10^{-4} & 34.12 & 30.46 \end{bmatrix}. \tag{4.12}$$

The corresponding optimal parameter set is

$$\hat{P}_c^{final} = \begin{bmatrix} 9.993 \times 10^{-5} & 2.000 \times 10^{-4} & 0.2498 & 0.2000 \end{bmatrix}, \tag{4.13}$$

which is very close to P_c^{correct} in equation (4.11), with the absolute error norm equal to 6.37×10^{-4}. With the identified values, the simulated responses are nearly identical to the original simulation results using the "correct" parameters.

From the output of the identification procedure, it was noted that the algorithm spent significant computing time searching for the appropriate v_1 and F_1 values, which form the slope of the rising stiction in low velocity regime. On the other hand, the determination of F_2 is easier as it is a constant and any velocity larger than v_2 provides a friction force of F_2.

Simplified Formulation and its Identification

For the sake of simplicity, the Classical model can be reduced to a two-parameter model by using an empirical relation

$$v_2 = 2v_1, \quad F_2 = 0.8F_1. \tag{4.14}$$

Thus, the parameter space for the optimization problem is now two-dimensional with constraints $v_1 > 0$ and $F_1 > 0$. According to (4.11), the correct parameter set for the *Simplified Classical model* is

$$P_{sc}^{\text{correct}} = [v_1^{\text{correct}} \quad F_1^{\text{correct}}] = [1 \times 10^{-4} \quad 0.25] \tag{4.15}$$

and the values of v_2 and F_2 can be calculated from equations (4.14) respectively. It is assumed that this modified 2-parameter model can save the computation time required for identification because of its simplicity.

With an arbitrarily chosen initial guess of $\hat{P}_{sc}^0 = [\ 0.1 \quad 0.1\ ]$, and by using the identification procedure introduced in §4.2.2, the final parameter set was evaluated as

$$\hat{P}_{sc}^{final} = [\ 1.000 \times 10^{-4} \quad 0.2502\ ],$$

which is very close to the correct values in (4.15).

Modified Formulation and its Identification

Another approach to modifying the Classical model for ease of parameter identification is to consider the slopes of the two linear regimes of the original Classical model and use the following substitutions:

$$s_1 = \frac{F_1}{v_1},\ s_2 = \frac{F_1 - F_2}{v_1 - v_2}. \tag{4.16}$$

This formulation of the *Modified Classical model* still has 4 parameters, which are

$$P_{mc} = [\ s_1 \quad s_2 \quad v_1 \quad v_2\ ].$$

The correct parameter set for this formulation, as interpreted from (4.11) with (4.16), is

$$P_{mc}^{\text{correct}} = [\ 2.5 \times 10^3 \quad -5 \times 10^2 \quad 1 \times 10^{-4} \quad 2 \times 10^{-4}\ ].$$

The following initial parameter set yields the optimal estimation for this model

$$\hat{P}_{mc}^0 = [\ 2.25 \times 10^2 \quad -44.45 \quad 2.25 \times 10^{-4} \quad 4.5 \times 10^{-4}\ ],$$

which in this case is

$$\hat{P}_{mc}^{final} = [\ 2.50 \times 10^3 \quad -500 \quad 1.00 \times 10^{-4} \quad 2.00 \times 10^{-4}\ ],$$

with the corresponding objective function equal to 4.98×10^{-4}.

4.3.2 Identification of Karnopp Model Parameters

Recall that Karnopp model is a three-parameter model with F_H representing the maximum stiction in the low velocity regime. In the simulated Karnopp model of the mass-spring example with

$$P_k^{correct} = [\ F_{slip} \quad F_H \quad D_v\ ] = [\ 0.2 \quad 0.25 \quad 2 \times 10^{-5}\ ],$$

F_H plays a minor role during the short 5-second simulation and was used only a few times to get the maximum stiction friction. This scarce usage makes the identification of F_H very difficult because the change in F_H has little effect on the simulation results.

On the other hand, the kinetic friction level F_{slide} plays a significant role and therefore can be identified very accurately. Following the identification procedure discussed in 4.2.4 with the initial parameter set as

$$\hat{P}_k^0 = [\ 0.3 \quad 0.5 \quad 5 \times 10^{-5}\ ],$$

the identified parameter set was calculated as:

$$\hat{P}_k^{final} = [\ 0.2000 \quad 0.5000 \quad 3.996 \times 10^{-5}\ ],$$

with the corresponding objective function equal to 4.96×10^{-4}.

4.3.3 Identification of Reset Integrator Model Parameters

The formulation of Reset Integrator Model was introduced in §2.3.3 and the simulation results were presented in §3.1.6. The Reset Integrator Model is a highly non-linear model and hence accurate parameter estimation was not achieved. The correct parameter values used in this model are

$$P_{ri}^{correct} = [\ 2 \times 10^4 \quad 0.25 \quad 30\ ],$$

while the optimal solution calculated with our optimization procedure was

$$\hat{P}_{ri}^{final} = [\ 4.713 \times 10^5 \quad 0.2024 \quad 0.7020\ ].$$

The numerical example considered in this section demonstrates that the optimization-based method can solve the parameter identification problem from the known relative motion at the contact point and corresponding friction. Sometimes the friction model needs to be reformulated for the sake of computational efficiency. The motion must be sensitive to the parameter being identified or satisfactory identification results can not achieved.

In the next chapter, the practical problem of contact friction parameter identification for the peg-hole insertion case is posed and formulated as an optimization problem. The similar non-linear approach to solving the parameter identification is discussed.

Chapter 5

Friction Parameter Identification from Experimental Data

5.1 Objective Function

As discussed in Chapter 1, the practical case for testing the proposed identification scheme was provided by the peg insertion experiments carried out on the UVic Robotics Test-bed. In this case, many variables were measured during the experiments, which were then used to calculate the friction force at the contact points. On the other hand, it is difficult to simulate the contact dynamics of the whole peg-hole insertion task to obtain the simulated relative motion at the contact points. Thus the objective function used for parameter identification for peg-hole insertion tests was formulated in the following form:

$$f(\hat{P}) = \left\| \mathbf{F}(\hat{P}) \ - \mathbf{F}^{\exp} \right\|, \tag{5.1}$$

where $\mathbf{F}$ is a vector of friction force values for the whole maneuver, sampled at 500Hz. The friction model used to calculate $\mathbf{F}(\hat{P})$ is the Modified Bristle model, which was introduced in §2.3.2 and will be discussed below. The parameters are to be identified for this model with the practical experimental data $\mathbf{F}^{\text{exp}}$.

The Modified Bristle model takes as its inputs the relative velocity at the contact points, and it computes the friction force as output. Thus, for parameter identification of the peg-in-hole insertions, the friction model is used to estimate the friction $\mathbf{F}(\hat{P})$ with the active parameter estimates $\hat{P}$. This calculation uses the measured position and relative velocity of the peg during its insertion into the hole. The values of friction force $\mathbf{F}^{\text{exp}}$ in the objective function (5.1) have not been measured directly, but can only be calculated by using the force measurements on the peg, the motion of the peg and the geometric constraints [24] [21].

5.2 Peg-hole Insertion Scenario

5.2.1 Experimental Measurement

The present data available to the identification project includes two parts: the dynamic variables obtained directly from the test-bed raw data, such as forces at the contact points of the peg and the walls of the hole, and variables estimated from above combined with quasi-equilibrium conditions and geometric constraint, such as positions and orientation of the peg.

The typical two-point contact during peg insertion into a hole is shown in Figure 5.1. The variables involved in friction identification include normal contact forces $\mathbf{F}_{na,b}$, tangential friction forces $\mathbf{F}_{fa,b}$ and relative displacements $X_{a,b}$ at the contact

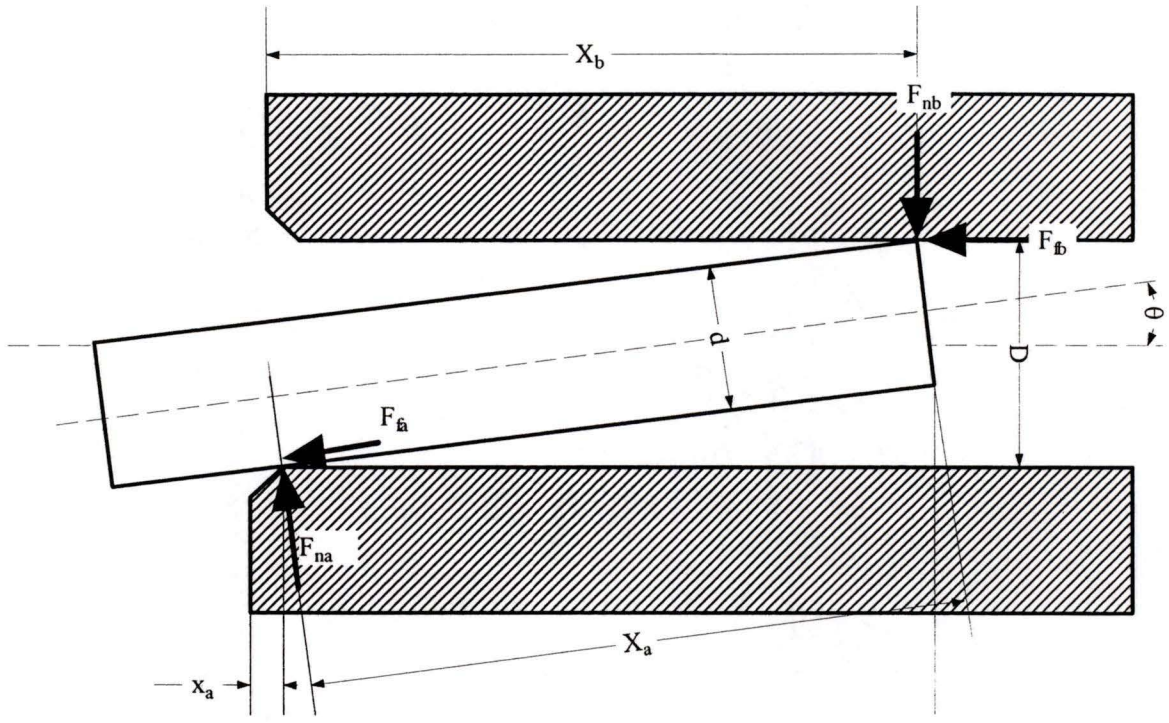

Figure 5.1: Two Point Contact During Peg Insertion into Hole

points "a" and "b", respectively. The identification scheme in this project focused on each contact point individually. Thus we investigate the friction parameter identification problem at contact point "a", and separately, at contact point "b".

To investigate the contact point "a", only contact variables at this point are used. These variables include X_a, $\dot{X}_a, \mathbf{F}_{fa}$, and $\mathbf{F}_{na}$ defined in Table 5.1 with each representing a vector of the corresponding values during the complete manoeuver. Of the above X_a, $\mathbf{F}_{na}$ and $\mathbf{F}_{fa}$ were measured or calculated from the position and force sensors, and $\dot{X}_a$ was obtained by the sixth-order differentiation of X_a. The reason $\dot{X}_a$ is needed is that in the bristle friction model, the relative velocity at a contact point is used to calculate the deflection of the bristle.

Table 5.1: Contact Variables at Point "a"

X_a	Relative displacement
$\dot{X}_a$	Relative velocity
$\mathbf{F}_{ta}$	Tangential force or friction froce
$\mathbf{F}_{na}$	Normal contact force reacting

In general, with relative velocity available it is possible to calculate the friction force during the time span with any given parameter set P, whether appropriate or not. With a minimization line search method, the parameter set which achieves the minimum discrepancy from the measured friction force can be obtained, i.e., for contact point "a" the objective function is defined as the discrepancy between friction force estimation $\hat{\mathbf{F}}_{fa}$ and the experimental value $\mathbf{F}_{fa}$. $\hat{\mathbf{F}}_{fa}$ is calculated from the dynamic variables with estimated parameter set P while $\mathbf{F}_{fa}$ is measured from experiments.

The complete peg-hole insertion test used to provide the experimental data for our estimation takes approximately 27 seconds and includes the following main stages:

Initial Point	t =-5s	peg is aligned flush against the right side of the hole.
Preparation	[-5—0s]	peg pulled out of the hole with prescribed misalignment.
Insertion	[0s—10s]	peg inserted into the hole at approximately 10 mm/s.
Removal	[10s—21s]	peg pulled out of the hole at approximately 10 mm/s.

According to the test-case profile, there was an one-second hold at the beginning of the Removal stage. As the Modified Bristle model we are using here is designed to treat stiction, it is reasonable to include the hold phase in the Removal stage without considering it separately. The hold phase is considered as the motion with zero velocity. The sampling frequency at which experimental data was collected is

500 Hz.

For the purpose of friction parameter identification, only data from the Insertion stage and the Removal stage during the whole test was used. Though there was peg manipulation during the Preparation stage, but it is not very important. In the following sections, the experimental data of test-case referred to as CDV022-5 is presented. This test-case is the most representative one among all the experiments carried out during the contact dynamics validation project. The test is carried out with a square steel peg with width 0.49", active RCC. The hole is adjustable and in this case it is set to 0.61" in width. The insertion task follows the procedure of four stages: *Depth sensor contact, Chamfer crossing(approach), One-point contact, and Two-point contact.* Detailed description of this test-case is included in Appendix B.

5.2.2 Friction Model Used for Simulation

The friction model used in MDSF to simulate the peg insertion manoeuver is revisited here. Recall this model was presented in §2.3.2 and referred to as the Modified Bristle model. Indeed, subsequent modifications of this model, not published in open literature, made the actual friction model used in MDSF very similar to the Reset Integrator Model, which was discussed in §2.3.3.

In the Reset Integrator model, the friction force is a function of relative velocity at the contact point and its integration. The Reset Integrator model has the same basic structure proposed in [4], combined with two more terms to include some features proposed by other researchers.

Here we present again the model used in MDSF by combining the original description of this model [4] with the additional features of the Reset Integrator Model.

The parameters of the model are $P = [\mu,\ k_f,\ \alpha,\ \beta]$, while the relative velocity $\mathbf{v}_r$ and the normal force $\mathbf{F}_n$ at the contact point are the necessary inputs to the model. The variables are the nominal bristle deflection $\mathbf{s}(t)$ and its resettable integrator $\dot{\mathbf{s}}(t)$, which is a function of $\mathbf{v}_r(t)$. The model is defined as follows:

$$
\begin{aligned}
s_{\max} &= \frac{\mu\,|\mathbf{F}_n|}{k_f} \\
\dot{\mathbf{s}} &= \begin{cases} 0, & \begin{cases} \text{if } \mathbf{v}_r > 0 \text{ and } |\mathbf{s}| \geq s_{\max} \\ \text{if } \mathbf{v}_r < 0 \text{ and } |\mathbf{s}| \leq -s_{\max} \end{cases} \\ \mathbf{v}_r, & \text{otherwise} \end{cases} \\
\mathbf{F}_f &= k_f\mathbf{s} + \beta\dot{\mathbf{s}} + \alpha k_f \mathbf{s}(|\mathbf{s}| < s_{\max})
\end{aligned}
$$

Comparing the above to the Modified Bristle model presented in §2.3.2, an additional component $\alpha k_f \mathbf{s}$ is included to generate the larger loads that can occur during stiction when. As well, a damping term $\beta\dot{\mathbf{s}}$ is included to account for damping when there is a short period of oscillation before sticking from higher velocity. During the identification procedure, the estimated friction force at k_{th} iteration $\hat{\mathbf{F}}_f^k$ is calculated by using the current state $[\mathbf{F}_n, \mathbf{v}_r, \mathbf{s}]$ and the estimated parameter set $P^k = [\mu^k,\ k_f^k,\ \alpha^k,\ \beta^k]$.

It should be noted that the experimental data collected during the previous project on contact dynamics validation [24] does not contain all the measurements required for friction parameter identification carried out in this research. The additional necessary inputs for the identification procedure were calculated by using the experimental data available. For example, the relative velocity at a contact point was obtained by differentiating the relative displacement at the contact point, which was measured during the experiment. (see Appendix B)

5.3 Identification Procedure

The identification procedure used to determine friction parameters for the MDSF friction model from peg insertion experimental data is shown in Figure 5.2. It incorporates the use of multiple initial configurations and optimization based numerical minimization as described in §4.2.2. The friction is evaluated according to the formulation of the Modified Bristle model implemented in MDSF.

In the identification procedure shown in Figure 5.2, the parameters are defined as follows:

n	number of friction parameters in the friction model,
i	index of the initial parameter set,
k_{max}	maximum number of optimization iterations,
k	index of optimization iterations,
ε	error tolerance.

The optimization problem was solved in MATLAB® by employing the Optimization Toolbox®, where synthesized minimizer searching methods were utilized for line search. Some of these methods are based on the Quasi-Newton line search algorithm, while some are adopted from other algorithms.

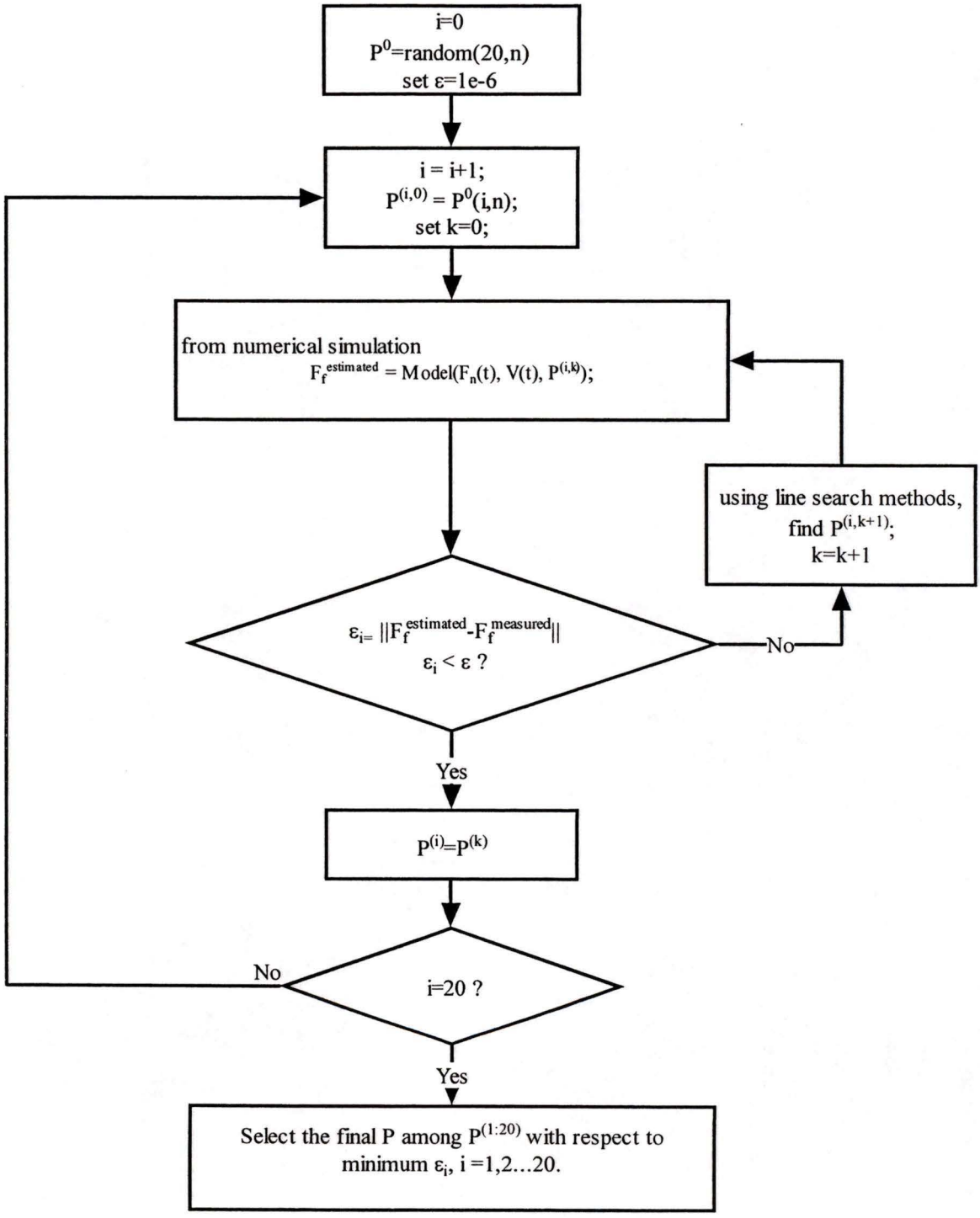

Figure 5.2: Identification Procedure from Experimental Data

5.4 Identification Results for MDSF Friction Model

It is foreseeable that the friction parameters might be different during different contact situations, i.e., different stages in the peg-hole tests. In this thesis, the Insertion stage and the Removal stage of the whole peg-hole insertion scenario are considered. During these stages, the relatively smooth two-point contact occurs.

The identification results about contact point "a" for the Insertion stage are listed in Table 5.2, and the results for the Removal stage are listed in Table 5.3. In each case, 20 randomly chosen initial parameter sets are employed in the optimization procedure to minimize the objective function in equation (5.1).

From Table 5.2, we observe that the estimated parameter set No. 1 yields the least value of the objective function, and it can be regarded as the best parameter set to match the experimental data for the Insertion stage of the manoeuver. In Table 5.3, the estimated parameter set No. 20 is the best among the 20 configurations. The two above-mentioned estimated parameter sets are cited below:

$$\hat{P}_1 = [0.345 \quad 5.79e3 \quad 83.8 \quad 0.273];$$

$$\hat{P}_2 = [0.242 \quad 1.80e5 \quad 35.1 \quad 0.362].$$

These two parameter sets are identified from different stages of the peg-hole insertion maneuver and they are quite different. The average of $\hat{P}_1$ and $\hat{P}_2$ was used as the initial guess for the optimization procedure with the objective function equal to the discrepancy of simulated friction and measured friction during both the Insertion and Removal stages. This yielded an optimal parameter set $\hat{P}_3$:

$$\hat{P}_3 = [0.255 \quad 1.85e5 \quad 67.9 \quad 0.278].$$

Table 5.2: Optimization Results for Point "a" for Insertion

	$f_{obj}(\hat{P}^{final})$	$\hat{P}^{final}$	$\hat{P}^{0}$
01	25.7	[0.345 5.79e3 83.8 2.73e-1]	[0.950 5.79e3 83.8 0.497]
02	26.2	[0.345 3.53e4 1.96 5.29e-1]	[0.231 3.53e4 1.96 0.900]
03	26.1	[0.344 8.13e4 68.1 1.00e-8]	[0.607 8.13e4 68.1 0.822]
04	29.4	[0.344 9.85e2 19.7 1.00e-8]	[0.486 9.86e2 37.9 0.645]
05	26.2	[0.345 1.39e4 83.2 1.00e-8]	[0.891 1.39e4 83.2 0.818]
06	26.1	[0.345 2.03e4 87.3 1.00e-8]	[0.762 2.02e4 50.3 0.660]
07	26.1	[0.345 1.99e4 88.9 1.00e-8]	[0.457 1.99e4 70.9 0.342]
08	26.1	[0.345 6.04e4 42.9 2.53e-2]	[0.019 6.04e4 42.9 0.290]
09	26.1	[0.345 2.72e4 30.5 5.18e-1]	[0.821 2.72e4 30.5 0.341]
10	26.15	[0.345 1.99e4 88.9 1.00e-8]	[0.445 1.99e4 19.0 0.534]
11	26.0	[0.347 7.00e3 103 1.00e-8]	[0.615 1.53e3 19.3 0.727]
12	26.1	[0.345 7.47e4 68.2 1.00e-8]	[0.792 7.47e4 68.2 0.309]
13	26.1	[0.345 4.45e4 30.3 5.37e-1]	[0.922 4.45e4 30.3 0.839]
14	26.1	[0.345 9.32e4 54.2 5.59e-1]	[0.738 9.32e4 54.2 0.568]
15	26.1	[0.345 4.66e4 15.1 6.36e-1]	[0.176 4.66e4 15.1 0.370]
16	26.1	[0.345 4.19e4 69.8 1.48e-1]	[0.406 4.19e4 69.8 0.703]
17	26.1	[0.345 8.46e4 37.8 5.05e-1]	[0.936 8.46e4 37.8 0.547]
18	26.1	[0.345 5.25e4 86.0 1.00e-8]	[0.917 5.25e4 86.0 0.445]
19	26.1	[0.345 2.03e4 85.4 1.00e-8]	[0.410 2.03e4 85.4 0.695]
20	26.1	[0.345 6.72e4 59.4 1.00e-8]	[0.894 6.72e4 59.4 0.621]

Table 5.3: Optimization Results for Point "a" for Removal

	$f_{obj}(\hat{P}^{final})$	$\hat{P}^{final}$	$\hat{P}^0$
01	496.8	[0.040 1.81e3 314 4.54]	[0.0084 1.59e3 0.67 28.7]
02	305.6	[0.235 7.47e4 0.68 1.13e-1]	[0.236 7.47e4 0.67 0.121]
03	283.8	[0.246 1.79e5 69.3 3.27e-1]	[0.236 4.45e4 1.58 0.0418]
04	297.9	[0.238 9.23e4 564 1.30e-1]	[0.236 9.32e4 35.5 0.154]
05	283.9	[0.245 1.77e5 138 3.31e-1]	[0.225 4.66e4 246 0.145]
06	320.2	[0.235 4.19e4 2.36 3.98e-2]	[0.236 4.19e4 2.27 0.0392]
07	302.2	[0.237 8.46e4 0.56 1.28e-1]	[0.235 8.46e4 0.52 0.136]
08	310.4	[0.240 5.27e4 649 2.99e-2]	0.235 5.25e4 0.89 0.0614]
09	324.8	[0.235 2.00e4 657 1.00e-8]	[0.234 2.03e4 2.42 0.00]
10	308.4	[0.235 6.72e4 0.67 9.89e-2]	[0.235 6.72e4 0.64 0.0989]
11	415.6	[0.127 5.78e3 1.11 9.71e-1]	[0.128 5.79e3 0.94 0.457]
12	283.9	[0.245 1.77e5 138 3.31e-1]	[0.020 3.53e4 0.01 8.000]
13	284.0	[0.245 1.76e5 156 3.30e-1]	[0.233 8.13e4 176 0.149]
14	526.2	[0.013 5.77e2 997 1.67]	[0.089 5.67e2 1.0e3 1.20]
15	326.2	[0.234 1.39e4 752 1.00e-8]	[0.221 1.39e4 0.99 0.00]
16	299.9	[0.239 8.47e4 616 1.05e-1]	[0.936 8.46e4 0.38 54.7]
17	310.4	[0.240 5.27e4 707 2.15e-2]	[0.917 5.25e4 0.86 44.5]
18	324.8	[0.236 2.02e4 644 1.00e-8]	[0.410 2.03e4 0.85 69.5]
19	305.5	[0.235 6.72e4 614 8.64e-2]	[0.894 6.72e4 0.59 62.1]
20	283.6	[0.242 1.80e5 35.1 3.62e-1]	[0.406 4.19e4 0.70 70.3]

Table 5.4: Comparison of Identified Parameters for Point "a"

Identified Friction parameters for point "a"	$\hat{P}_1$	$\hat{P}_2$	$\hat{P}_3$
μ	0.345	0.242	0.255
k_r	5.79e3	1.80e5	1.85e5
β	83.8	35.1	67.9
α	0.273	0.362	0.278
Error at the Insertion stage	25.7	77.6	71.2
Error at the Removal stage	660	284	285

Thus $\hat{P}_3$ is regarded as the final identified parameter set that minimizes the discrepancy of the simulated response and the experimental data for the whole peg-hole insertion scenario. The three identified parameter sets are listed for comparison in Table 5.4.

The simulated friction forces calculated with the above three parameter sets and the experimental data are shown in Figure 5.3. The accuracy of the identified friction coefficient μ is satisfactory. As can be seen from these results, $\hat{P}_3$ provides the best match between simulated and experimental friction forces. The identified parameter values can be considered quite accurate since they provide a simulated response sufficiently close to the measured friction.

The same procedure is applied to identify contact friction parameters at the contact point "b". Since the contact geometry at point "a" and point "b" are different, the friction parameters are expected to be different. The identified results are listed in Table 5.5 for the Insertion stage and Table 5.6 for the Removal stage.

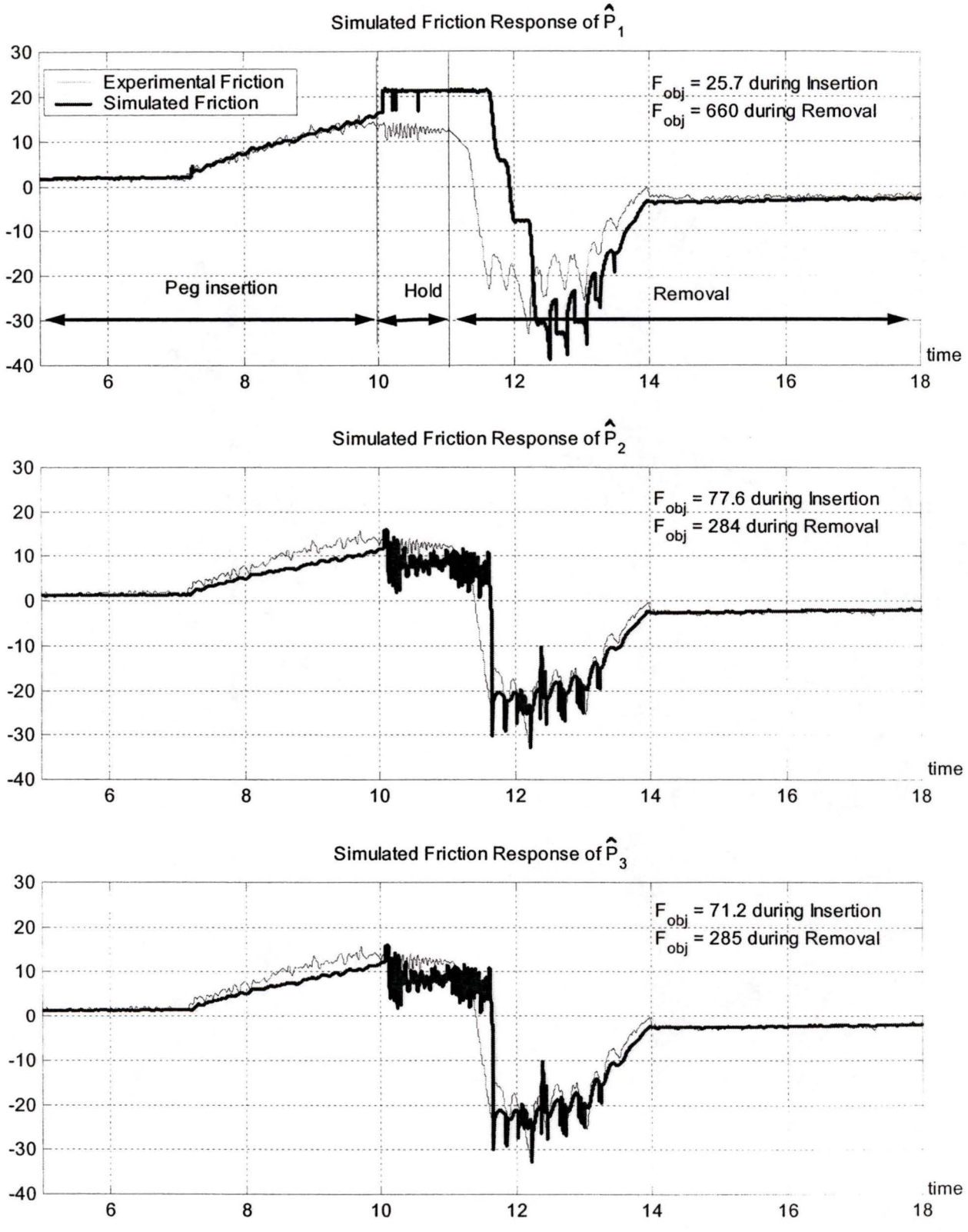

Figure 5.3: Estimated and Measured Friction

Table 5.5: Optimization Results for Point "b" for Insertion

#	$f_{obj}(\hat{P}^{final})$	$\hat{P}^{final}$	$\hat{P}^{0}$
01	36.0	[0.297 5.79e4 83.8 0.497]	[0.950 5.79e4 83.8 0.497]
02	36.0	[0.297 3.53e5 1.96 0.900]	[0.231 3.53e5 1.96 0.900]
03	36.0	[0.297 8.13e5 68.1 0.822]	[0.607 8.13e5 68.1 0.822]
04	36.0	[0.297 9.86e3 37.9 0.645]	[0.486 9.86e3 37.9 0.645]
05	36.0	[0.297 1.39e5 83.2 0.818]	[0.891 1.39e5 83.2 0.818]
06	36.0	[0.297 2.03e5 50.3 0.660]	[0.762 2.03e5 50.3 0.660]
07	36.0	[0.297 1.99e5 70.9 0.342]	[0.456 1.99e5 70.9 0.342]
08	36.0	[0.297 6.04e5 42.9 0.290]	[0.0185 6.04e5 42.9 0.290]
09	36.0	[0.297 2.72e5 30.5 0.341]	[0.821 2.72e5 30.5 0.341]
10	36.0	[0.297 1.99e5 19.0 0.534]	[0.445 1.99e5 19.0 0.534]
11	36.0	[0.297 1.53e4 19.3 0.727]	[0.615 1.53e4 19.3 0.727]
12	36.0	[0.297 7.47e5 68.2 0.309]	[0.792 7.47e5 68.2 0.309]
13	36.0	[0.297 4.45e5 30.3 0.838]	[0.922 4.45e5 30.3 0.838]
14	36.0	[0.297 9.32e5 54.2 0.568]	[0.738 9.32e5 54.2 0.568]
15	36.0	[0.297 4.66e5 15.1 0.370]	[0.176 4.66e5 15.1 0.370]
16	36.0	[0.297 4.19e5 69.8 0.703]	[0.406 4.19e5 69.8 0.703]
17	36.0	[0.297 8.46e5 37.8 0.547]	[0.935 8.46e5 37.8 0.547]
18	36.0	[0.297 5.25e5 86.0 0.445]	[0.917 5.25e5 86.0 0.445]
19	36.0	[0.297 2.03e5 85.4 0.695]	[0.410 2.03e5 85.4 0.695]
20	36.0	[0.297 6.72e5 59.4 0.621]	[0.894 6.72e5 59.4 0.621]

Table 5.6: Optimization Results for Point "b" for Removal

#	$f_{obj}(\hat{P}^{final})$	$\hat{P}^{final}$	$\hat{P}^0$
01	396	[0.298 1.05e5 842 1.66e-4]	[0.95 5.79e4 83.8 0.497]
02	401	[0.303 2.71e5 860 1e-8]	[0.231 3.53e5 1.96 0.9]
03	489	[0.342 8.13e5 66.2 1e-8]	[0.607 8.13e5 68.1 0.822]
04	378	[0.187 9.86e3 38 0.0299]	[0.486 9.86e3 37.9 0.645]
05	401	[0.301 2.75e5 822 1e-8]	[0.891 1.39e5 83.2 0.818]
06	401	[0.301 2.75e5 822 1e-8]	[0.762 2.03e5 50.3 0.66]
07	401	[0.301 2.75e5 822 1e-8]	[0.456 1.99e5 70.9 0.342]
08	463	[0.287 6.04e5 1e-8 1e-8]	[0.0185 6.04e5 42.9 0.29]
09	401	[0.3 2.72e5 836 1e-8]	[0.821 2.72e5 30.5 0.341]
10	406	[0.275 1.99e5 1e3 1e-8]	[0.445 1.99e5 19 0.534]
11	327	[0.262 1.53e4 667 1e-8]	[0.615 1.53e4 19.3 0.727]
12	477	[0.315 7.47e5 1 1e-8]	[0.792 7.47e5 68.2 0.309]
13	402	[0.316 3.19e5 704 1e-8]	[0.922 4.45e5 30.3 0.838]
14	521	[0.39 9.32e5 54.2 1e-8]	[0.738 9.32e5 54.2 0.568]
15	401	[0.3 2.76e5 776 1e-8]	[0.176 4.66e5 15.1 0.37]
16	418	[0.348 4.19e5 69.8 1e-8]	[0.406 4.19e5 69.8 0.703]
17	497	[0.355 37.8 8.46e5 1e-8]	[0.935 8.46e5 37.8 0.547]
18	401	[0.301 2.75e5 822 1e-8]	[0.917 5.25e5 86 0.445]
19	405	[0.276 2.03e5 1e3 1e-8]	[0.41 2.03e5 85.4 0.695]
20	468	[0.3 6.72e5 1e-8 1e-8]	[0.894 6.72e5 59.4 0.621]

5.5 Discussion of Results

5.5.1 Comparison to Previous Results

Two previous projects conducted in the Space and Subsea Robotics Laboratory at the University of Victoria by Van Vliet and Sharf [24], and Sharf and Crawford [21] attempted identification of the friction coefficient by using experimental data collected during the peg-hole insertion tests.

In the validation project [24], the coefficient of sliding friction μ_k between peg and hole, both made of steel, was identified from a set of one-point contact experiments. The coefficient of friction was calculated from the ratio of axial to lateral forces, which in turn correspond to tangential and normal forces at the contact point:

$$\mu_k = \frac{F_f}{F_n}.$$

The average value calculated for steel was obtained as:

$$\mu_{k,steel} = 0.22 \pm 10\%.$$

The coefficient of static friction was not identified separately in that study but was set to 1.2 times the corresponding kinetic friction coefficient. The uncertainty in the estimated nominal values of μ_k was 10% for steel.

Sharf and Crawford [21] carried out a comprehensive estimation of both the coefficient of kinetic and static friction. They investigated different ways of calculating μ_k, e.g., by using contact forces at individual contact points, or alternatively by using forces measured at the force sensor only. Their identification results obtained from the same peg-hole insertion test as used in this thesis are presented in Table 5.7, where we include μ values at the two contact points during Insertion (In) and

Table 5.7: The Previous Results of Friction Coefficient

Test Case CDV022-5				
Insertion	μ_a In	$\sigma(\mu_a$ In)	μ_b In	$\sigma(\mu_b$ In)
	0.33	0.05	0.29	0.03
Removal	μ_a Out	σ (μ_a Out)	μ_b Out	σ (μ_b Out)
	0.26	0.03	0.37	0.07

Removal (Out) of the maneuver. The standard deviation of the results (σ) are also presented. μ_k has values at different contact point during different insertion scenario. It can be observed that the values in Table 5.7 for two-point contact are somewhat higher than the estimate obtained in [24] for one-point contact.

The identification results from the current thesis yield a value of 0.26 for the coefficient of sliding friction at the contact point "a" and a value for static friction 28% higher (as $\alpha = 0.28$). These are in the range of the previously estimated values for μ. As well, our procedure identifies other parameters of the friction model, in particular the bristle stiffness $k_r = 1.85e6$ and damping coefficient $\beta = 67.9$.

For contact point "b", an average value of 0.30 is obtained for the coefficient of sliding friction.

5.5.2 Error Sources

It is appropriate to comment on the error source which corrupt the identification results. Errors in our identification procedure can arise from several sources:

(1) Friction measurement errors.

As is generally the case and as is the case in the peg-hole contact dynamics

interface on the Robotics Test-bed at UVic, it is not feasible to measure normal and tangential contact forces at individual contact points (except during one point contact). The only means to obtain these force values for the peg-hole setup is by using static-equilibrium conditions with geometric constraints and measurements of forces on the walls. However, the peg is not moving with a strictly constant velocity and the inertial force in small value is ignored.

(2) Modelling errors.

According to the MDSF friction model used in our parameter identification procedure, the different parameters cannot be identified with the same weight. The parameters to which the motion is sensitive can be determined thoroughly, i.e., it is easy for the line search algorithm to find their exact values. However, parameters that have little direct effect on the measured experimental variables cannot be identified or cannot be identified precisely.

Chapter 6

Conclusions

The first major effort of this thesis involved a comprehensive review and analysis of different friction models, with the goal of understanding the structure and features of friction phenomenon. Friction models developed throughout history, including the most recent research results, are examined. The friction models are used in the simulations of a simple mass-spring system and a multiple mass-spring system to verify their capability of capturing non-linear friction characteristics.

The second major effort of this thesis deals directly with an identification scheme based on numerical optimization, which is first synthesized from analytical algorithms in the relevant literature and then used to post-process the experimental data and to extract the values of friction parameters in various models. The identification scheme has been proven valid and effective to solve the parameter identification problem by using a simple numerical example and the practical experimental case. Friction parameters identified from experimental data will provide users of MDSF the necessary input for contact friction and thus assist in the use of MDSF for simulation and validation of space manipulator operations involving contact tasks.

6.1 Modelling and Simulation

This thesis presents a comprehensive investigation of friction models and their simulation performance at low velocities. The major conclusions of the friction model investigation are as follows:

1. For modeling friction, three types of traditional static friction models — the Classical model, Karnopp model, and 7-parameter model — and three modern dynamic friction models — the Bristle model, Reset Integrator model, and Modified Bristle model were compared. It was noted that the earlier models can only include basic friction features. With the application of computer technology to friction simulation, further development of friction models must address the issue of computational efficiency.

2. From the simulation results of above-mentioned friction models for a simple mass-spring system moving on a rough surface, it was observed that every friction model presents a reasonable response of frictional behavior in the slow velocity regime. This proves that all models considered are capable of capturing frictional characteristics and simulating contact friction at low velocity.

3. Among the models considered, the Reset Integrator model is the most efficient one in computation. The Modified Bristle model proposed by MD Robotics and implemented in MDSF has a similar formulation to the Reset Integrator model, and comprises its extension to the more general three dimensional case.

6.2 Parameter Identification of Friction Models

The previous project Contact Dynamics Validation of MDSF was conducted on the UVic Robotics test-bed and a large amount of experimental data was generated. In this thesis, an optimization-based nonlinear parameter identification method was proposed to solve the contact friction parameter identification problem. The data was post-processed to extract the necessary information for parameter identification of Modified Bristle model employed by MDSF. The identification procedure was presented, and the identification results were discussed and compared to the previous results from other approaches.

The parameter identification method was designed, but is not limited to, identification of friction parameters in non-linear relationships. It can be generalized to identify any kind of system parameters which cannot be determined directly, when the numerical model of the system is available.

The major conclusions on parameter identification are as follows:

1. It is noted that in the recent contact tasks, the robot manipulator is very rigid regarding the fulfillment of the desired trajectory. Small change in tangential contact friction force has little effect on the overall motion response. Due to the weak sensitivity, it is difficult to estimate the contact friction from the motion response. The friction force is also difficult to measure directly. Thus a reliable means to precisely determine contact friction is necessary to further perform friction parameter identification.

2. It was demonstrated in this thesis that a numerical optimization method can be implemented off-line to determine non-trivial parameter values from experimen-

tal data collected during contact dynamics experiments. The contact friction force calculated with the identified parameters was compared to the friction force measured during the experiments. The comparison results indicate that the optimization-based parameter identification algorithm is a suitable approach for estimating the contact friction parameters.

3. Based on the fact that by minimizing the discrepancy between the estimated friction force and the experimental friction force we can solve the friction parameter identification problem, the development of an **on-line** parameter identification strategy using a similar algorithm is suggested. For an on-line scheme, the problems of reliability, stability, and efficiency need to be considered.

4. The Modified Bristle model used in MDSF was further verified with the newly identified friction parameters. The estimated contact friction force showed a good agreement with the corresponding experimental measurement.

5. Friction parameter identification in contact dynamics of robotic peg-hole insertion tasks makes practical sense because it can provide the users of MDSF necessary input to execute simulations of space station manipulations. Furthermore, the effective friction parameters along with other contact dynamic parameters will help MDSF in validating space station operations involving contact tasks.

6.3 Future Work

In much of the literature, the difficult problem of friction coefficient identification is noted. However, it has been shown that it can be solved off-line by a specially designed

optimization algorithm. For the ongoing research of on-line parameter identification, a scale-down optimization solution with limited number of iteration steps at each time step was attempted but was not successful.

There are several issues that need to be addressed in order to the on-line minimization scheme:

(1) The optimization solution must be calculated in a single sampling period, which can be inadequate for a fully functional optimization procedure, so the number of iterations must be limited. The newer computational platforms have increased the computation efficiency dramatically, which will alleviate this constraint.

(2) The necessary input to optimization method, including contact friction and relative velocity at the contact point, must be measured or estimated in some way. This can be done by solving for the geometry of the contacting objects. The peg-hole insertion task, which is a two dimensional, two contact point case is easy to solve, but for a more complex contact task with more contact points, the geometry can be a difficult to solve.

On the other hand, adaptive controllers have been developed to track damping and stiffness effects during contact robotics manipulation. For the contact dynamics parameter identification, one approach is to use a force tracking scheme implemented in an adaptive controller. It is expected that the parameters being estimated will converge to their actual levels under some periodic excitation. This method was proposed by Seraji [19] and at least proven to be valid for estimation of contact stiffness and contact damping, which have linear relationships with the relative motion at the contact point [9]. For contact friction, which is a highly nonlinear case, this adaptive control method needs some adaptation. We emphasize that the system response does

not have a linear relationship to the input parameters. Thus the adaptive control variables involved with friction can only be obtained by the scale-down optimization solution, instead on a system matrix, which is valid for damping and stiffness. Some research results are available on addressing the use of adaptive control methods for friction compensation in mechanism systems. They may be helpful in developing the on-line friction identification scheme for robotic manipulation as well.

Investigation of the relationship of traditional static models and the integration-based dynamic models is also necessary. If some friction parameters are proven to be exchangeable, it will be easier and more straightforward for parameter identification with complex friction models.

References

[1] B. Armstrong-Helouvry, P. Dupont, and C. Canudas de Wit. A survey of models, analysis tools and compensation methods for the control of machines with friction. *Automatica*, 30:1083–1138, 1994.

[2] E. A. Avallone and T. Baumeister III. *Marks' Standard Handbook for Mechanical Engineers – 9th Edition.* McGraw-Hill, 1987.

[3] F. P. Bowden and D. Tabor. *Friction and Lubrication.* Methuen, 1967.

[4] Q. Chen and G. R. Tomlinson. Parametric identification of systems with dry friction and non-linear stiffness using a time series model. *ASME Journal of Vibration and Acoustics*, 118:252–263, 1996.

[5] K. C. Cheok, H. Hu, and N. K. Loh. Modelling and identification of a class of servomechanism systems with stick-slip friction. *Transactions of the ASME*, 110:324–328, 1988.

[6] P. R. Dahl. A solid friction model. *TOR 158(3107-18), The Aerospace Corporation, EI Segundo, CA*, 1968.

[7] C. Canudas de Wit and H. Olsson. A new model for control of systems with friction. *IEEE Transactions on Automatic Control*, 40:419–425, 1995.

[8] H. Du and S. S. Nair. Identification of friction for control at low velocities. *Proceedings of the American Control Conference, Albuquerque, NM,*, pages 2289–2293, 1997.

[9] D. Erickson. Contact stiffness and damping estimation for constrained robotic systems. Master's thesis, University of Victoria, 2000.

[10] M. Gäfvert. Comparison of two friction models. Master's thesis, Lund Institute of Technology, 1996.

[11] Jr. D. A. Haessig and B. Frieland. On the modelling and simulation of friction. *ASME Journal of Dynamic Systems, Measurement, and Control*, 113:354–362, 1991.

[12] J. Y. Jeon, S. W. Lee, H. K. Chae, and J. H. Kim. Low velocity friction identification and compensation using accelerated evolutionary programming. *Proc. International Conference on Evolutionary Computation*, 5:372–377, 1996.

[13] D. Karnopp. Computer simulation of stick-slip friction in mechanical dynamic systems. *ASME Journal of Dynamics Systems, Measurement, and Control*, 107:100–103, 1985.

[14] J. H. Kim, H. K. Chae, J. Y. Jeon, and S. W. Lee. Identification and control of systems with friction using accelerated evolutionary programming. *IEEE Control Systems*, 16(4):38–47, 1996.

[15] S. W. Lee and J. H. Kim. Friction identification using evolution strategies and robust control of positioning tables. *ASME Journal of Dynamic Systems, Measurement, and Control*, 121:619–624, 1999.

[16] O. Ma, K. Buhariwala, N. Roger, J. Maclean, and R. Carr. Mdsf - a generic development and simulation facility for flexible, complex robotic systems. *Robotica*, 15:49–62, 1997.

[17] H. Olsson, K. J. Åström, C. Canudas de Wit, M. Gäfvert, and P. Lischinsky. Friction models and friction compensation. *European Journal of Control*, (4):176–195, 1998.

[18] Ladislao Reti. Leonardo on bearings and gears. *Scientific American*, 224(4):110–100, 1971.

[19] H. Seraji and R. Colbaugh. Force tracking in impedance control. *The Int. Journ. of Robotics Research*, 16(1):97–117, 1997.

[20] Lawrence F. Shampine and Mark W. Reichelt. The MATLAB ODE suite. *SIAM journal on scientific computing: a publication of the Society for Industrial and Applied Mathematics*, 18(1), 1997.

[21] I. Sharf and C. Crawford. Investigation of contact parameters from constrained robotic tasks: Estimation of coefficient of friction. Technical report, University of Victoria, 1999.

[22] J. E. Shigley and C. R. Mischke. *Standard Handbook of Machine Design, 2nd Edition.* McGraw-Hill, 1996.

[23] J. Van Vliet and I Sharf. Experimental investigations of contact tasks for space-based manipulators: Further validation of mdsf contact dynamics capabilities. Technical report, University of Victoria, 1999.

[24] J. Van Vliet and I. Sharf. Experimental validation of contact dynamics simulation of constrained robotic tasks. Technical report, University of Victoria, 1999.

[25] P. Wild, J. Jeswiet, and T. Moore. Development of an embedded friction sensor for metal forming applications. Technical report, Queen's University, 2000.

[26] B. Yao and M. Tomizuka. Adaptive robust motion and force tracking control of robot manipulators in contact with compliant surfaces with unknown stiffness. *Transactions of ASME*, 120:232–239, 1998.

Appendix A

Abbreviations Notation and Symbols

α	Stiction bonus or stiction gradient
β	Dampling coefficient, viscous friction coefficient
γ	Temporal parameter of the rising static friction in the 7-parameter model
δ_i	Deflection of the i_{th} bristle in the Bristle model
δ_v	Viscous friction index
δ_s	Snapping point
Δ	New bristle range
ε	Error, difference or discrepancy
μ	Friction coefficient
μ_k	Kinetic friction coefficient
σ	Standard deviation
σ_0	Stiffness coefficient in the LuGre model
σ_1	Damping coefficient in the LuGre model
σ_2	Viscous friction coefficient in the LuGre model

τ_L	Time constant of frictional memory in the 7-parameter model
b_A	Upper bristle position at point A
b_i	Upper bristle position of the i_{th} bristle
D_v	Velocity bound, parameter in the Karnopp model
f_{obj}	Objective function
E_i	Input energy
E_k	Kinetic energy
E_p	Peak energy
E_s	Strain energy
F	Force
$\mathbf{F}(\bullet)$	Mapping function values of friction in vector form
F_1	Stiction in the Classical model
F_2	Sliding friction in the Classical model
F_c	Coulomb friction force in the 7-parameter model
F_e	External applied force
$\mathbf{F}_{est}$	Estimation of fricton force
F_f	Instaneous friction force
$\mathbf{F}_{fa}$, $\mathbf{F}_{fa}$	Instaneous friction force at point "a" or "b"
$\mathbf{F}_f$	Three dimensional friction force vector
F_H	Maximum stiction in the Karnopp model
F_k	Kinetic friction force
F_n	Normal contact force
$\mathbf{F}_n$	Three dimensional normal contact force vector
$\mathbf{F}_{na}$	Normal force reacting at point "a"

F_s	Static friction, or stiction
F_S	Stribeck friction in the 7-parameter model
$F_{S,a}$	Stribeck friction of the previous sliding period in the 7-parameter model
$F_{S,\infty}$	Stribeck friction after a long time at rest in the 7-parameter model
$\mathbf{F}_{sam}$	Sampled Friction from experimental data
F_{slip}	Sliding friction in the Karnopp model
F_{ss}	Friction force at steady state
$\mathbf{F}_{ta}$	Tangential force at point "a"
F_v	Viscous friction in the 7-parameter model and other models
$g(v)$	Positive function in the LuGre model
i	Bristel index in the Bristle model;
$K,\ K_1,\ K_2$	Stiffness of a piece of spring
k_b	Bristle Stiffness in the Bristle model
$k_f,\ k_r$	Bristle Stiffness or spring rate of the bristle
k_t	tangential stiffness in the 7-parameter model
k_{max}	Maximum number of iterations for optimization.
$m,\ m_1,\ m_2$	Mass
n, N	Number of bristles in the Bristle model
n_{max}	Maximum number of initial configurations
p, s	Bristle deflection
$\dot{p}$	Differential of the bristle deflection
p_0, s_{max}	Maximum bristle deflection
P	Parameter set
$\hat{P}$	Estimated parameter set
$\hat{P}^0$	Initial parameter estimate

$\hat{P}^k$	Estimated Parameter set at k_{th} iteration in a optimization procedure
P_7	Parameter set of 7-parameter model
$P_c,\ \hat{P}_c$	Parameter set of Classical model and its estimation
$P_k,\ \hat{P}_k$	Parameter set for the Karnopp model and its estimation
$P_{mc},\ \hat{P}_{mc}$	Parameter set of the Modified Classical model and its estimation
$P_{ri},\ \hat{P}_{ri}$	Parameter set for the Reset Integrator model and its estimation
$P_{sc},\ \hat{P}_{sc}$	Parameter set of the Simplified Classical model and its estimation
$\mathbf{s}$	Three dimensional bristle deflection vector
$\dot{s}$	Derivative of bristle deflection
s_{max}, p_0	Maximum bristle deflection
t	Time
t_2	Dwell time, or duration of time at zero velocity in the 7-parameter model
v_0	Input velocity in the simple mass-spring example
v_1	Parameter in the Classical model
v_2	Parameter in the Classical model
v, v_r	Relative velocity
v_S	Stribeck velocity in the LuGre model
$\mathbf{v}_t$	Three dimensional tangential velocity vector
W	Work
x_0	Input displacement in the simple mass-spring example
x_A	Lower bristle position around point "a"
X_a	Displacement at contact point "a"
$\dot{X}_a$	Relative velocity at contact point "a"
X_b	Displacement at contact point "b"

$\dot{X}_b$	Relative velocity at contact point "b"
$\mathbf{X}$	System response of motion vector
$\mathbf{X}(\bullet)$	Mapping function values in vector form
$X(\bullet)$	Mapping function to simulated motion
$X_F(\bullet)$	Mapping function to simulated friction
$\mathbf{X}_F$	System response of of friction vector
$\hat{\mathbf{X}}_F$	Vector of estimated friction
x_i	Lower bristle position around the i_{th} bristle
$\dot{x}_s$	Characteristic velocity of the Stribeck friction in the 7-parameter model
x_r	Relative position (displacement)
z	Average deflection of bristles in the LuGre model
z_{ss}	Average deflection of bristles at steady-state in the LuGre model

Appendix B

Peg-Hole Insertion Task

For a typical peg-hole insertion task, as shown in Figure B.1, the following insertion stages are defined (adapted from [24]):

- *No Contact:* The peg is fully removed from the hole; there is no contact between peg and hole profiles or the ram of the depth-of-insertion sensor.
- *Depth Sensor Contact (approach):* Although the peg is still not contacting the hole profiles, it is pushing against the ram of the depth-of-insertion sensor. The peg remains in contact with the depth-of-insertion sensor throughout Chamfer Crossing, One-Point Contact, and Two-Point Contact.
- *Chamfer Crossing:* The corner of the peg (or possibly the tip of a chamfered peg) is in contact with the RHS chamfer of the hole fixture.
- *One-Point Contact:* The RHS edge of the peg is in contact with the root of the chamfer on the RHS of the hole.
- *Two-Point Contact:* In addition to the one-point contact between the RHS edge

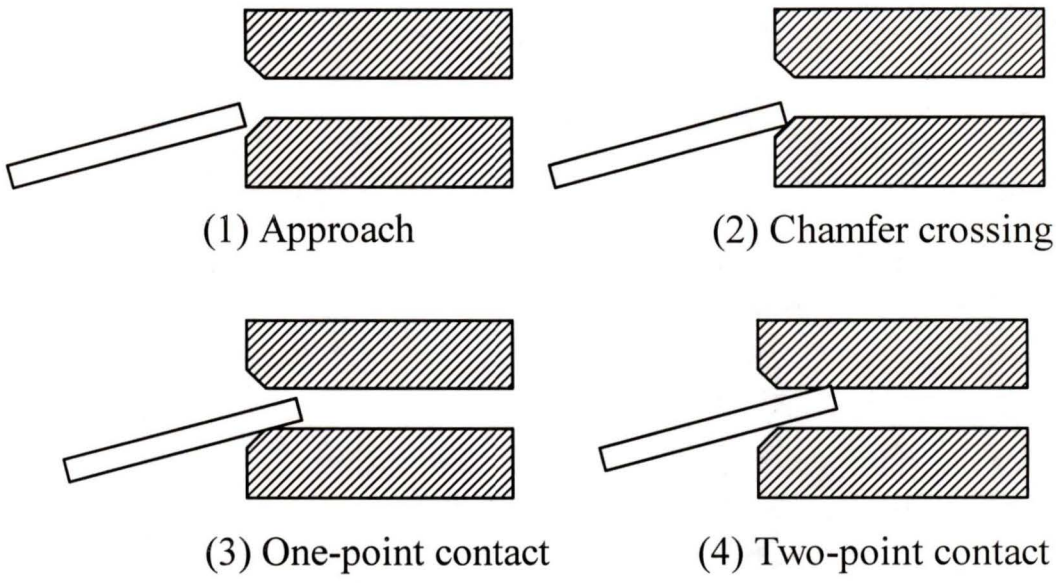

Figure B.1: Peg-hole Insertion Stages

of the peg and the root of chamfer on the RHS of the hole, the LHS front corner of the peg (or LHS root of the peg chamfer) is in contact with the face of the LHS hole profile.

During the contact dynamics validation project, a number of different experiments were examined. Test-case CDV022-5 is a representative example. The CDV022 test-case lasts 21 seconds, starting with a 10 second insertion phase, followed by a 1 second hold and a 10 second removal.

Both the peg and hole are made of steel. The width of the peg is 0.49", and the width of the hole D is adjustable and for this test case it is set to 0.61".

The geometry relation of two point contact during the peg-hole insertion task is show in Figure B.2. Given the measured depth of insertion of the peg, h^*, and the peg angle θ (evaluated from kinematics). It is possible to calculate the axial location

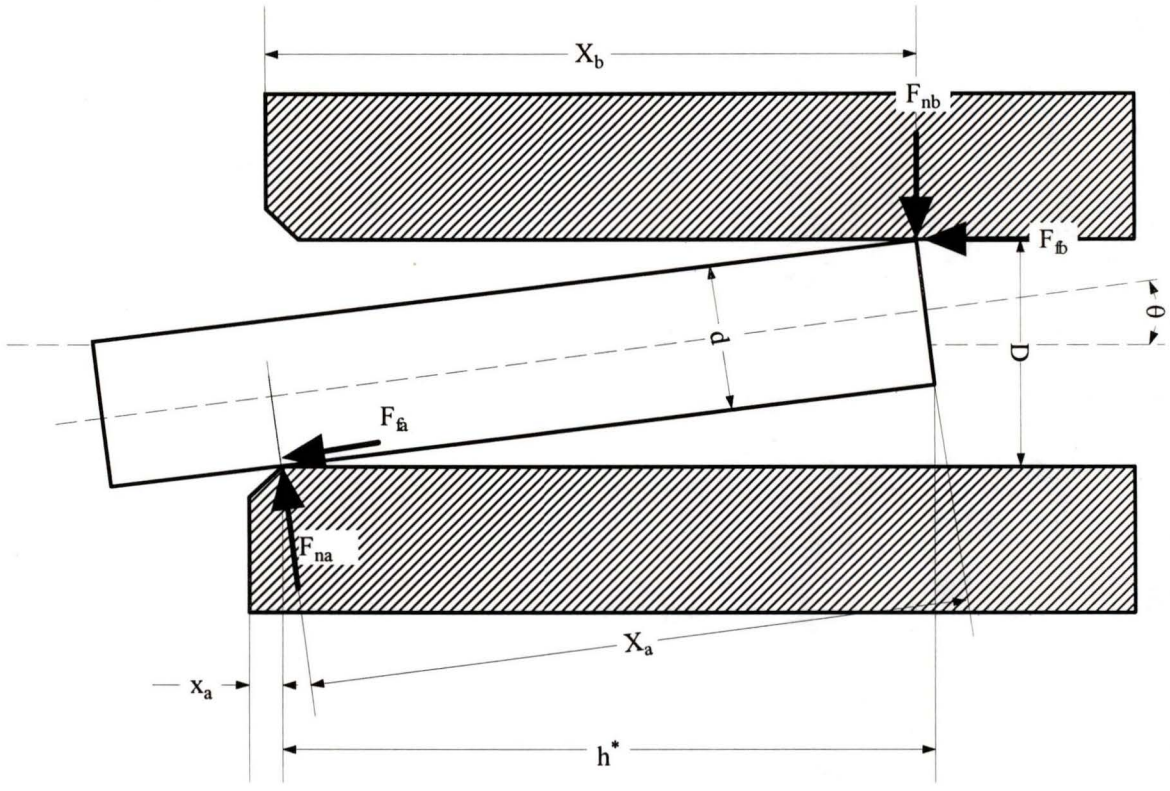

Figure B.2: Contact Dynamics for Peg-Hole Insertion Task

of the two contact points as follows:

$$\begin{aligned} X_a &= h^* - d\sin\theta, \\ X_b &= \frac{h^* - x_a}{\cos\theta}. \end{aligned}$$

Thus the relative velocities at each contacting point at

$$\begin{aligned} v_a &= \dot{X}_a = \frac{dX_a}{dt}, \\ v_b &= \dot{X}_b = \frac{dX_b}{dt}. \end{aligned}$$

The above were calculated numerically by using numerical differentiation method.

Vita

Surname: Lin **Given Names:** Alec

Place of Birth: Beijing, China
Date of Birth: June 22, 1972

Educational Institutions Attended:

Beijing Polytechnic University	1992 to 1997

Degrees Awarded:

B. Sc in Engineering	Beijing Polytechnic University	1997

Honours and Awards:

Advanced Systems Institute Fellowship	1998
University of Victoria Fellowship	1998 to 1999
Award of Excellent Student of Beijing Higher Institute	1997

Partial Copyright License

I hereby grant the right to lend my thesis to users of the University of Victoria Library, and to make single copies only for such users or in response to a request from the Library of any other university, or similar institution, on its behalf or for one of its users. I further agree that permission for extensive copying of this thesis for scholarly purposes may be granted by me or a member of the University designated by me. It is understood that copying or publication of this thesis for financial gain shall not be allowed without my written permission.

Title of Thesis:

Friction Identification From Robotic Insertion Tasks

Author 

Alec Lin
May 6, 2001